variety of the eight-electron systems. The relative stabilities of the six-electron and eight-electron systems are probably influenced more by the nature of the core ligands, i.e., the μ_3 and μ_2 groups or atoms, than by the remaining nine ligand atoms, but we do not yet know what the important factors are. It will be necessary to obtain and study further examples of both the six-electron and eight-electron types before this relationship can be understood.

Acknowledgment. We thank the U. S. National Science Foundation and the U. S.-Israeli Binational Science Foundation for support.

(23) Shibahara, T.; Hattori, H.; Kuroya, H. *J. Am. Chem. Soc.* **1984**, *106*, 2710.

Registry No. $[Mo_3(CCH_3)(O_2CMe)_3Br_3(H_2O)_3]ClO_4$, 95344-37-9; $[Mo_3(CCH_3)(O_2CMe)_3Br_3(H_2O)_3]ClO_4 \cdot 4H_2O$, 95344-38-0; $Mo_2(O_2CCH_3)_4$, 14221-06-8; $[Mo_3(CCH_3)_2(O_2CMe)_6(H_2O)_3]^+$, 95344-39-1; $Mo(CO)_6$, 13939-06-5.

Supplementary Material Available: Tables of structure factors and anisotropic thermal parameters, details of the X-ray work, and a stereoview of the unit cell contents (23 pages). See any current masthead page for ordering information.

Unique Bonding and Geometry in η-Cyclopentadienyltantalum–Diene Complexes. Preparation, X-ray Structural Analyses, and EHMO Calculations

Hajime Yasuda,[1a] Kazuyuki Tatsumi,[1a] Takuji Okamoto,[1a] Kazushi Mashima,[1a] Keonil Lee,[1a] Akira Nakamura,*[1a] Yasushi Kai,[1b] Nobuko Kanehisa,[1b] and Nobutami Kasai*[1b]

Contribution from the Department of Macromolecular Science, Faculty of Science, Osaka University, Toyonaka, Osaka 560, and Department of Applied Chemistry, Faculty of Engineering, Osaka University, Suita, Osaka 565, Japan. *Received September 25, 1984*

Abstract: From the 1:1 reactions of tetrachloro(cyclopentadienyl)tantalum or tetrachloro(pentamethylcyclopentadienyl)tantalum ($LTaCl_4$, L = Cp, Cp*) with a series of (2-butene-1,4-diyl)magnesiums, six kinds of tantalum–mono(diene) complexes of the formulation $CpTaCl_2$(diene) or Cp^*TaCl_2(diene) were isolated as air-sensitive purple crystals and characterized by their NMR and mass spectra as well as by X-ray analysis. $CpTaCl_2$(butadiene) crystallizes in space group $P2_1/n$ with a = 6.615 (1) Å, b = 10.962 (1) Å, c = 14.384 (2) Å, β = 97.02 (1)°, and Z = 4. Pertinent bond distances are C(1)–C(2) = 1.458 (16), C(2)–C(3) = 1.375 (16) Å, Ta–C(1) = 2.258 (12) Å, and Ta–C(2) = 2.424 (11) Å. The dihedral angle between the C(1)–Ta–C(4) and C(1)–C(2)–C(3)–C(4) planes is 94.9°. These data support the view that the complex assumes the novel bent metallacyclopent-3-ene structure. Six kinds of bis(diene) complexes of the type $LTa(diene)_2$ (L = Cp, Cp*) including mixed-diene complexes were also prepared in a similar manner and isolated as air-sensitive yellow crystals. $CpTa(2,3\text{-dimethylbutadiene})_2$ belongs to the orthorhombic space group *Pnma* with a = 8.947 (1) Å, b = 12.291 (2) Å, c = 13.512 (2) Å, and Z = 4. The two diene ligands assume a unique geometrical conformation; one of the dienes lies supine and the other prone looking with the Cp ring upward. $Cp^*Ta(2,3\text{-dimethylbutadiene})_2$ crystallizes in space group $P2_1$ with a = 10.468 (2) Å, b = 12.442 (2) Å, c = 8.020 (1) Å, β = 106.68 (2)°, and Z = 2. The plane of one of the dienes is nearly parallel to the Cp* ring, the dihedral angle being 18.5°, while the plane of the other diene makes a dihedral angle of 83.5° with the Cp* ring. Extended-Hückel calculations revealed that the observed orientation of the butadiene ligand in $CpTaCl_2(C_4H_6)$ (lying supine) is 15.7 kcal more stable than the geometrical isomer where the butadiene lying prone is coordinated to metal. Among the three structures considered for $CpTa(butadiene)_2$, the observed structure is computed to be the most stable, 28.4 kcal more stable than the supine–supine geometry where the two dienes are oriented toward the Cp ring and 23.3 kcal more stable than another isomer (prone–prone) where the CH_2 groups at the diene termini are pointed away from the Cp ring.

In recent years the chemistry of metal–diene complexes has entered a new phase with the advent of highly reactive group 4[4-8] metal–diene complexes such as Cp_2M(diene) (M = Ti, Zr, Hf) which furnish the synthetically useful selective carbon–carbon bond-forming reactions, reflecting their polar M–C bondings.[2-4] They react not only with alkenes, dienes, and alkynes but also with carbonyl compounds such as aldehydes, ketones, and esters with extremely high regioselectivity. Their structural pattern is also unique and the s-trans coordination of a diene to a mononuclear metal complex has first been found in this field with Zr and Hf complexes.[5,6] The X-ray and NMR analyses of the s-cis isomers of zirconium–1,3-diene complexes revealed that they have the novel bent metallacyclopent-3-ene structure (**1**) in which the dihedral angle between the planes defined by C(1), M, C(4) and C(1), C(2), C(3), C(4) atoms are greater than 90° and the C(2)–C(3)

(1) (a) Faculty of Science. (b) Faculty of Engineering.

(2) (a) Yasuda, H.; Kajihara, Y.; Mashima, K.; Nagasuna, K.; Nakamura, A. *Chem. Lett.* **1981**, 671. (b) Yasuda, H.; Kajihara, Y.; Nagasuna, K.; Mashima, K.; Nakamura, A. *Ibid.* **1981**, 719. (c) Kai, Y.; Kanehisa, N.; Miki, K.; Kasai, N.; Mashima, K.; Nagasuna, K.; Yasuda, H.; Nakamura, A. *Ibid.* **1982**, 1979. (d) Akita, M.; Yasuda, H.; Nakamura, A. *Ibid.* **1983**, 217. (e) Kai, Y.; Kanehisa, N.; Miki, K.; Kasai, N.; Akita, M.; Yasuda, H.; Nakamura, A. *Bull. Chem. Soc. Jpn.* **1983**, *56*, 3735.

(3) (a) Fischer, M. B.; James, E. J.; McNeese, T. J.; Nyburg, S. C.; Posin, B.; Wong-Ng, W.; Wreford, S. S. *J. Am. Chem. Soc.* **1980**, *102*, 4941. (b) Beatty, R. P.; Datta, S.; Wreford, S. S. *Inorg. Chem.* **1979**, *18*, 3139.

(4) (a) Skibbe, V.; Erker, G. *J. Organomet. Chem.* **1983**, *241*, 15. (b) Erker, G.; Dorf, U. *Angew. Chem. Suppl.* **1983**, 1120. (c) Erker, G.; Engel, K.; Atwood, J. L.; Hunter, W. E. *Angew. Chem., Int. Ed. Engl.* **1983**, *22*, 494.

(5) (a) Erker, G.; Wicher, J.; Engel, K.; Rosenfeldt, F.; Dietrich, W.; Krüger, C. *J. Am. Chem. Soc.* **1980**, *102*, 6346. (b) Yasuda, H.; Kajihara, Y.; Mashima, K.; Nagasuna, K.; Lee, K.; Nakamura, A. *Organometallics* **1982**, *1*, 388; **1983**, *2*, 478. (c) Kai, Y.; Kanehisa, N.; Miki, K.; Kasai, N.; Mashima, K.; Nagasuna, K.; Yasuda, H.; Nakamura, A. *J. Chem. Soc., Chem. Commun.* **1982**, 191. (d) Yasuda, H.; Nagasuna, K.; Akita, M.; Lee, K.; Nakamura, A. *Organometallics* **1984**, *3*, 1470.

(6) Benn, R.; Schroth, G. *J. Organomet. Chem.* **1982**, *228*, 71.

0002-7863/85/1507-2410$01.50/0

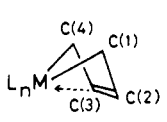

1

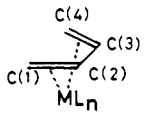

2

bond is significantly shorter than C(1)–C(2) and C(3)–C(4) bonds.[7] The vast majority of the diene complexes reported so far have the *s-cis*-η^4-1,3-diene structure (**2**) having bond lengths of C(2)–C(3) ≥ C(1)–C(2) [C(3)–C(4)] and M–C(1) ≥ M–C(2), the dihedral angles of which are generally acute, <90°.

The marked contrast in structure and reactivity observed between the group 4 metal–diene and the group 8–10 metal–diene complexes prompted us to explore the synthesis of the corresponding tantalum–diene complexes to clarify the chemistry distinctive to the group 5 metal–diene complexes. This paper describes the preparative method, structural features, and a Hückel MO rationalization on the unique bondings and the orientation of the dienes observed in tantalum–diene complexes of the type $LTaCl_2$(diene) and $LTa(diene)_2$, where L is the η^5-cyclopentadienyl (Cp) or η^5-pentamethylcyclopentadienyl (Cp*) group.[8]

Experimental Section

General Remarks. All operations were conducted with Schlenk techniques under an argon atmosphere. Tetrahydrofuran and hexane were dried over Na/K alloy, distilled, and degassed before use. Tetrachloro(cyclopentadienyl)tantalum ($CpTaCl_4$)[9a] and tetrachloro(pentamethylcyclopentadienyl)tantalum (Cp^*TaCl_4)[9b] were obtained by the established routes starting from $CpSnBu_3$ or Cp^*SnBu_3. Bifunctional magnesium reagents, (2-butene-1,4-diyl)magnesium and its higher homologues, were prepared by the reported procedure.[10] ^{1}H NMR (100 MHz) spectra were recorded on a Varian XL-100 instrument and analyzed with a Varian spin simulation program. ^{13}C NMR (22.5 MHz) spectra were recorded on a JEOL FX-90Q instrument. Electronic spectra were obtained on a Jasco Model UVIDEC-5A spectrometer and the mass spectra (EI) on a JEOL O1SG-2 (low-resolution) or a JEOL DX-300 (exact mass) spectrometer at 70 eV.

Preparation of (η-C_5H_5)$TaCl_2$(butadiene) (3). A suspension of (2-butene-1,4-diyl)magnesium (3.1 mmol) in THF (5 mL) was dropwise added over a 30-min period to $CpTaCl_4$ (1.5 g, 3.8 mmol) dissolved in a mixture of THF (50 mL) and HMPA (1 mL) at −30 °C. The mixture was stirred at −20 °C for 1 h and then evaporated to dryness. The product was extracted from the residue into two portions of oxygen-free hexane (40 mL) at 50 °C. After salts were separated by centrifugation using a specially designed two-necked tube, the hexane solution was concentrated to 9 mL and cooled to −20 °C to give $CpTaCl_2(C_4H_6)$ (**3**) as purple crystals; yield, 42%. Single crystals submitted for X-ray analysis were obtained by recrystallization from hexane, after the sample was purified by sublimation at 65 °C (10^{-4} torr): mp 70 °C; high-resolution mass spectrum (intensity ratio), *m/e* 373.9636 (0.7, calcd for $CpTaC_4H_6{}^{37}Cl_2$ 373.9696), 371.9676 (4.1, calcd for $CpTaC_4H_6{}^{35}Cl^{37}Cl$ 371.9665) 369.9715 (6.3, calcd for $CpTaC_4H_6{}^{35}Cl_2$ 369.9695), 320 (10.6, $CpTa^{37}Cl_2$), 318 (64.5, $CpTa^{35}Cl^{37}Cl$), 316 (100.0 $CpTa^{35}Cl_2$); UV (THF, $\lambda_{max}(\epsilon)$) 383 (290), 560 (40) nm. Anal. Calcd for $C_9H_{11}TaCl_2$: C, 29.13; H, 2.99. Found: C, 28.89; H, 3.40. NMR data are given in Table I.

$CpTaCl_2$(isoprene) (**4**) and $CpTaCl_2$(2,3-dimethylbutadiene) (**5**) were prepared in a similar manner starting from (2-methyl-2-butene-1,4-diyl)magnesium or (2,3-dimethyl-2-butene-1,4-diyl)magnesium and isolated as purple crystals in 50% or 56% yield, respectively.

For **4**: mp 123 °C; mass spectrum (intensity ratio), *m/e* 388 (0.8, $CpTaC_5H_8{}^{37}Cl_2$), 386 (5.3, $CpTaC_5H_8{}^{35}Cl^{37}Cl$), 384 (7.1, $CpTaC_5H_8{}^{35}Cl_2$), 320 (12.0, $CpTa^{37}Cl_2$), 318 (66.2, $CpTa^{35}Cl^{37}Cl$), 316 (100.0, $CpTa^{35}Cl_2$); UV (THF, $\lambda_{max}(\epsilon)$) 375 (210), 550 (30) nm. Anal. Calcd for $C_{10}H_{13}Cl_2Ta$: C, 31.20; H, 3.40. Found: C, 30.58; H, 3.81.

For **5**: mp 133 °C; mass spectrum (intensity ratio), *m/e* 402 (0.2, $CpTaC_6H_{10}{}^{37}Cl_2$), 400 (2.4, $CpTaC_6H_{10}{}^{35}Cl^{37}Cl$), 398 (4.1, $CpTaC_6H_{10}{}^{35}Cl_2$); UV (THF, $\lambda_{max}(\epsilon)$) 380 (260), 553 (50) nm. Anal. Calcd for $C_{11}H_{15}Cl_2Ta$: C, 33.11; H, 3.79. Found: C, 33.11; H, 3.89.

Preparation of (η-C_5Me_5)$TaCl_2$(diene) (6–8). To a stirred THF solution (20 mL) of Cp^*TaCl_4 (1.1 g, 2.4 mmol) was added a suspension of (2-butene-1,4-diyl)magnesium (2.0 mmol) in THF (5 mL) at −20 °C. The solution was allowed to warm to 20 °C, stirred there for 1 h and evaporated to dryness. The product was extracted with hot hexane at 50 °C and the extract was concentrated to 5 mL and cooled to −20 °C to give purple crystals of Cp^*TaCl_2(butadiene) (**6**) in 66% yield. Further purification was performed by sublimation at 110 °C (10^{-4} torr), mp 215 °C; mass spectrum (intensity ratio), *m/e* 444 (0.6, $Cp^*TaC_4H_6{}^{37}Cl_2$), 442 (3.3, $Cp^*TaC_4H_6{}^{35}Cl^{37}Cl$), 440 (5.2, $Cp^*TaC_4H_6{}^{35}Cl_2$), 390 (1.1, $Cp^*Ta^{37}Cl_2$), 388 (65.6, $Cp^*Ta^{35}Cl^{37}Cl$), 386 (100.0, $Cp^*Ta^{35}Cl_2$); UV (THF, $\lambda_{max}(\epsilon)$) 350 (3800), 550 (60) nm. Anal. Calcd for $C_{14}H_{22}Cl_2Ta$: C, 38.12; H, 4.80. Found: C, 39.58; H, 5.09. NMR data are given in Table I.

Similarly prepared in 75% yield by reaction of (2-methyl-2-butene-1,4-diyl)magnesium (1.75 mmol) with Cp^*TaCl_4 (0.8 g, 1.75 mmol) was Cp^*TaCl_2(isoprene) (**7**): mp 138 °C; mass spectrum (intensity ratio), *m/e* 458 (0.2, $Cp^*TaC_5H_8{}^{37}Cl_2$), 456 (1.1, $Cp^*TaC_5H_8{}^{35}Cl^{37}Cl$), 454 (1.6, $Cp^*Ta^{35}Cl_2$), 390 (1.1, $Cp^*Ta^{37}Cl_2$), 388 (64.5, $Cp^*Ta^{35}Cl^{37}Cl$), 386 (100.0, $Cp^*Ta^{35}Cl_2$); UV (THF, λ_{max} (ϵ)) 345 (1300), 544 (50) nm. Anal. Calcd for $C_{15}H_{23}TaCl_2$: C, 39.58; H, 5.09. Found: C, 39.85; H, 5.55.

The corresponding 2,3-dimethylbutadiene complex, Cp^*TaCl_2(2,3-dimethylbutadiene) (**8**), was prepared by the same procedure: mp 130 °C; mass spectrum (intensity ratio), *m/e* 472 (0.3, $Cp^*TaC_6H_{10}{}^{37}Cl_2$), 470 (1.5, $Cp^*Ta^{35}Cl^{37}Cl$), 468 (2.2, $Cp^*Ta^{35}Cl_2$); UV (THF, $\lambda_{max}(\epsilon)$) 350 (2500), 530 (60) nm. Anal. Calcd for $C_{10}H_{25}TaCl_2$: C, 40.96; H, 5.37. Found: C, 39.37; H, 6.41.

Preparation of (η^5-C_5H_5)Ta(diene)$_2$ (9–10). To a stirred suspension of $CpTaCl_4$ (2.2 g, 5.7 mmol) in THF (15 mL) was added a suspension of (2-butene-1,4-diyl)magnesium (11.3 mmol) at −78 °C. The mixture was allowed to warm to room temperature. After being stirred for 2 h, the solution was evaporated to dryness and oxygen-free hexane (50 mL) was added to the residue. The salt was removed by centrifugation under an argon atmosphere. Then the supernatant solution was concentrated to 5 mL and cooled to −20 °C to induce the precipitation of yellow crystals of Cp Ta(butadiene)$_2$ (**9**): yield, 62%; mp 135 °C; high-resolution mass spectrum (intensity ratio), *m/e* 354.0801 (24.0, calcd for $CpTaC_8H_{12}$, 354.0787), 300 (21.3, $CpTaC_4H_6$), 296 (66.2, $CpTaC_4H_6 - H_4$), 272 (100.0, $CpTaC_4H_6 - C_2H_4$), 246 (53.2, CpTa); UV (THF, $\lambda_{max}(\epsilon)$) 335 (1600) nm. Anal. Calcd for $C_{13}H_{17}Ta$: C, 44.09; H, 4.80. Found: C, 43.85; H, 4.90. NMR data are given in Table III.

(η-C_5H_5)Ta(2,3-dimethylbutadiene)$_2$ (**10**) was obtained by essentially the same procedure as described for **9** and isolated as orange crystals in 63% yield: mp 188 °C; mass spectrum (intensity ratio), *m/e* 410 (30.8, $CpTaC_{12}H_{20}$), 328 (16.5, $CpTaC_6H_{10}$), 324 (100.0, $CpTaC_6H_{10} - H_4$), 296 (30.1, $CpTaC_6H_{10} - C_2H_4$); UV (THF, $\lambda_{max}(\epsilon)$) 370 (1800) nm. Anal. Calcd for $C_{17}H_{25}Ta$: C, 49.77; H, 6.14. Found: C, 49.38; H, 6.35.

Preparation of (η-C_5Me_5)Ta(diene)$_2$ (11–13). To a THF solution of Cp^*TaCl_4 (1.2 g, 2.6 mmol) cooled to −78 °C was added a suspension of (2-butene-1,4-diyl)magnesium (5.2 mmol) in THF (5 mL). The mixture was allowed to warm to room temperature, stirred there for 1 h, and evaporated to dryness. The hexane extract was concentrated to 5 mL and cooled to 0 °C to give orange crystals of Cp*Ta(butadiene)$_2$ (**11**) in 54% yield: mp 56 °C; ^{1}H NMR (C_6D_6, 30 °C) 4.98 (m, 2, CH), 4.18 (m, 2, CH), 2.10 (m, 2, CH_2(syn)), 1.70 (m, 2, CH_2(syn)), 0.92 (m, 2, CH_2(anti)), 0.00 (m, 2, CH_2(anti)); high-resolution mass spectrum (intensity ratio), *m/e* 424.1570 (53.5, calcd for $Cp^*TaC_8H_{12}$, 424.1569), 370 (69.2, $Cp^*TaC_4 - H_6$), 368 (100, $Cp^*TaC_4H_6 - H_2$), 366 (32.1, $Cp^*TaC_4H_6 - H_2$); UV (THF, $\lambda_{max}(\epsilon)$) 320 (1300), 385 (600) nm. Anal. Calcd for $C_{18}H_{27}Ta$: C, 50.95; H, 6.41. Found: C, 50.68; H, 5.85.

(η-C_5Me_5)Ta(isoprene)$_2$ (**12**) was prepared in the same manner in 65% yield as yellow viscous semisolid: ^{1}H NMR (C_6D_6) 4.79 (m, 1, CH), 4.24 (m, 1, CH), 2.16 (m, 2, CH_2(syn)), 1.94 (m, 2, CH_2(syn)), 0.98 (m, 2, CH_2(anti)), 0.19 (m, 2, CH_2(anti)), 1.98, 2.07 (m, 6, CH_3); mass spectrum (intensity ratio), *m/e* 452 (5.3, $Cp^*TaC_{10}H_{16}$), 384 (85.2, $Cp^*TaC_5H_8$), 380 (100), $Cp^*TaC_5H_8 - H_4$), 356 (7.5, $Cp^*TaC_5H_8 - C_2H_4$). Anal. Calcd for $C_{20}H_{31}Ta$: C, 53.10; H, 6.91. Found: C, 52.65; H, 7.25.

(η-C_5Me_5)Ta(2,3-dimethylbutadiene)$_2$ (**13**) was similarly isolated as orange crystals in 82% yield: mp 132 °C; mass spectrum (intensity ratio), *m/e* 480 (1.7, $Cp^*TaC_{12}H_{20}$), 398 (86.3, $Cp^*TaC_6H_{10}$), 394 (100, $Cp^*TaC_6H_{10} - H_4$), 370 (8.2, $Cp^*TaC_6H_{10} - C_2H_4$), 354 (40.3, $Cp^*TaC_6H_{10} - C_3H_8$). Anal. Calcd for $C_{20}H_{31}Ta$: C, 55.00; H, 7.34. Found: C, 55.06; H, 7.38.

(7) (a) Erker, G.; Wicher, J.; Engel, K.; Krüger, C. *Chem. Ber.* **1982**, *115*, 3300. (b) Erker, G.; Engel, K.; Krüger, C.; Chiang, A.-P. *Ibid.* **1982**, *115*, 3311. (c) Erker, G.; Engel, K. *Organometallics* **1984**, *3*, 128.

(8) For a preliminary report: Yasuda, H.; Mashima, K.; Okamoto, T.; Nakamura, A. "Proceedings of the Eleventh International Conference on Organometallic Chemistry", Atlanta, GA, 1983, Abstr. 79.

(9) (a) Bunker, M. J.; De Cian, A.; Green, M. L. H.; Moreau, J. J. E.; Siganporia, N. *J. Chem. Soc., Dalton Trans.* **1980**, 2155. (b) Herrmann, W. A.; Kalcher, W. W.; Biersack, H.; Bernal, I.; Creswick, M. *Chem. Ber.* **1981**, *114*, 3558.

(10) (a) Fujita, K.; Ohnuma, Y.; Yasuda, H.; Tani, H. *J. Organomet. Chem.* **1976**, *113*, 201. (b) Yasuda, H.; Nakano, Y.; Natsukawa, K.; Tani, H. *Macromolecules* **1978**, *11*, 586. See also ref 5b.

Synthesis of Mixed Diene Complex 22. Method A. A suspension of (2-butene-1,4-diyl)magnesium (1 mmol) was added to a stirred solution of Cp^*TaCl_2 (2,3-dimethylbutadiene) (0.5 g, 1 mmol) at −78 °C. The mixture was stirred at room temperature for 1 h and then evaporated to dryness. The product was extracted into hexane (40 mL) and recrystallized at −20 °C to give Cp^*Ta(butadiene)(2,3-dimethylbutadiene) in 70% yield.

Method B. To a solution of Cp^*TaCl_2(butadiene) (0.23 g, 0.6 mmol) in THF (5 mL) was added at −78 °C a THF solution of (2,3-dimethyl-2-butene-1,4-diyl)magnesium (0.6 mmol) with a magnetic stirring. After the solvent was removed by trap-to-trap distillation, the product was extracted into hexane (30 mL) and purified by recrystallization at −20 °C to give Cp^*Ta(butadiene)(2,3-dimethylbutadiene) in 75% yield as orange crystals.

Spectral data, melting point, and elemental analysis for the complex obtained by the method A are identical with those obtained by the method B: mp 123 °C; high-resolution mass spectrum (30 eV, intensity ratio) m/e 452.1881 (100.0, calcd for $Cp^*TaC_{10}H_{16}$ 452.1882), 398 (59.5, $Cp^*TaC_6H_{10}$), 394 (91.5, $Cp^*TaC_6H_{10} - H_4$), 370 (44.5, $Cp^*TaC_4H_6$ and $Cp^*TaC_6H_{10} - C_2H_4$), 366 (28.8, $Cp^*TaC_4H_6 - H_4$); UV (THF, $\lambda_{max}(\epsilon)$) 385 (400) nm. Anal. Calcd for $C_{20}H_{31}Ta$: C, 53.10; H, 6.91. Found: C, 53.05; H, 6.99.

Crystallographic Data. All X-ray experiments were carried out on a Rigaku automated four-circle diffractometer with Zr-filtered or graphite-monochromatized Mo Kα radiation. The unit-cell parameters at 20 °C were determined by a least-squares fit to 2θ values of 20, 30, and 34 strong higher angle reflections for **3**, **10**, and **13**, respectively.

$CpTaCl_2$(butadiene) (**3**): monoclinic, $P2_1/n$, a = 6.615 (1) Å, b = 10.962 (1) Å, c = 14.348 (2) Å, β = 97.02 (1)°, U = 1032.6 (2) Å^3, Z = 4, D_{calcd} = 2.386 g cm^{-3}, $F(000)$ = 688, μ (Mo Kα) = 109.9 cm^{-1}. CpTa(2,3-dimethylbutadiene)$_2$ (**10**): orthorhombic, $Pnma$, a = 8.947 (1) Å, b = 12.291 (2) Å, c = 13.512 (2) Å, U = 1486.0 (4) Å^3, Z = 4, D_{calcd} = 1.834 g cm^{-3}, $F(000)$ = 800, μ (Mo Kα) = 72.9 cm^{-1}. Cp^*Ta(2,3-dimethylbutadiene)$_2$ (**13**): monoclinic, $P2_1$, a = 10.468 (2) Å, b = 12.442 (2) Å, c = 8.020 (1) Å, β = 106.68 (2)°, U = 1000.6 (3) Å^3, Z = 2, D_{calcd} = 1.594 g cm^{-3}, $F(000)$ = 480, μ (Mo Kα) = 54.2 cm^{-1}.

Collection and Reduction of Intensity Data. The X-ray diffraction data were measured by using crystals with dimensions of 0.45 × 0.20 × 0.10 mm, 0.45 × 0.35 × 0.30 mm, and 0.45 × 0.30 × 0.25 mm for **3**, **10**, and **13**, respectively. Two types of X-ray generator were used for the experiments: conventional type (40 kV, 30 mA) for **3**; rotating anode type (40 kV, 200 mA) for **10** and **13**. The integrated intensities were measured by the θ–2θ scan technique at a 2θ scan rate of 4° min^{-1} for **3** and 8° min^{-1} for **10** and **13**. The scan width was $\Delta 2\theta = (2.0 + 0.70 \tan\theta)°$. The background intensities were measured at both ends of a scan for 5 s (**3** and **13**) or for 4 s (**10**). No significant intensity decay of the standard reflections was observed for any of the crystals used. The number of intensities collected up to 2θ of 75° was 5425, 4029, and 3971 for **3**, **10**, and **13**, respectively; the number of reflections with $[|F_o| > 3\sigma(F_o)]$ was 3876, 3206, and 3462, respectively. The intensity data were corrected for the usual Lorentz and polarization effects, but an absorption correction[11] was applied only for **3** where the crystal dimensions were nonuniform.

Determination and Refinement of the Structure. The crystal structures of **3**, **10**, and **13** were solved by the conventional heavy-atom method. The crystal structures were refined by the full-matrix least-squares method as implemented in the X-RAY SYSTEM and using the observed reflections only $[|F_o| > 3\sigma(F_o)]$. After anisotropic refinement of the non-hydrogen atoms, all hydrogen atoms except methyl hydrogens were located in the difference Fourier maps with the help of geometrical calculations and were refined isotropically for **3** and **10**. However, attempts to find the hydrogen atoms for **13** were unsuccessful. The weighting function used in the final stages of the refinements was $w = [\sigma^2(F_o) + 0.003(F_o)^2]^{-1}$. The final R (R_w) indices are 0.048 (0.073), 0.061 (0.079), and 0.049 (0.062) for **3**, **10**, and **13**, respectively. The accuracy of the molecular structure of **13** at 20 °C has not been improved significantly by redetermination of the structure at −60 °C (R = 0.059, R_w = 0.070).[12] Hereafter all discussions of **13** are based on the data collected at 20 °C.

All calculations were carried out on an ACOS S900 computer at the Crystallographic Research Center, Institute for Protein Research, Osaka University.

Molecular Orbital Calculations. All calculations were of the extended-Hückel type, with weighted H_{ij}'s.[13] The valence state ionization potentials, H_{ii}, of Ta 5d, 6s, and 6p orbitals were taken from those of V 3d, 4s, and 4p orbitals, respectively, obtained by Kubacek et al.[14] The Basch and Gray orbitals[15] were used for the Ta functions. The Rh parameters are those given by Summerville and Hoffmann.[16] The parameters for C and H atoms are standard ones.

The extended-Hückel parameters are as follows. H_{ii}: Ta 6s, −8.81 eV; Ta 6p, −5.52 eV; Ta 5d, −11.0 eV; Rh 5s, −8.09 eV; Rh 5p, −4.57 eV; Rh 4d, −12.5 eV; H 1s, −13.6 eV; C 2s, −21.4 eV; C 2p, −11.4 eV. Orbital exponents: Ta 6s, 2.280; Ta 6p, 2.241; Ta 5d, 4.762 (0.6600) + 1.938 (0.5592); Rh 5s, 2.135; Rh 5p, 2.100; Rh 4d, 4.29 (0.5807) + 1.97 (0.5685); H 1s, 1.3; C 2s, 2p, 1.625.

Assumed geometries not given in the text are as follows. $CpTaCl_2(C_4H_6)$ and $CpTa(C_4H_6)_2$: C–C(butadiene), 1.44 Å; C–C–C(butadiene), 120°; C–C(Cp), 1.40 Å; C–H, 1.09 Å; Ta–Cp (centroid), 2.12 Å; Ta–m, 1.7934 Å; Ta–Cl, 2.40 Å. $RhCl(C_4H_6)_2$: Rh–Cl, 2.45 Å; Rh–m, 1.5285 Å. The point m is defined in **27**, which sits in the butadiene plane at φ = 0° and is at the middle point of the line connecting C_1 and C_4 when L = 0.0 Å.

Results and Discussion

Synthesis. (a) Tantalum–Mono(diene) Complexes. With the advent of reactive new bifunctional organomagnesium reagents,[10] a series of new tantalum–diene complexes, $CpTaCl_2$(diene) and Cp^*TaCl_2(diene), has first been prepared according to the reaction shown in eq 1. The addition of 0.9 equiv of (2-butene-1,4-

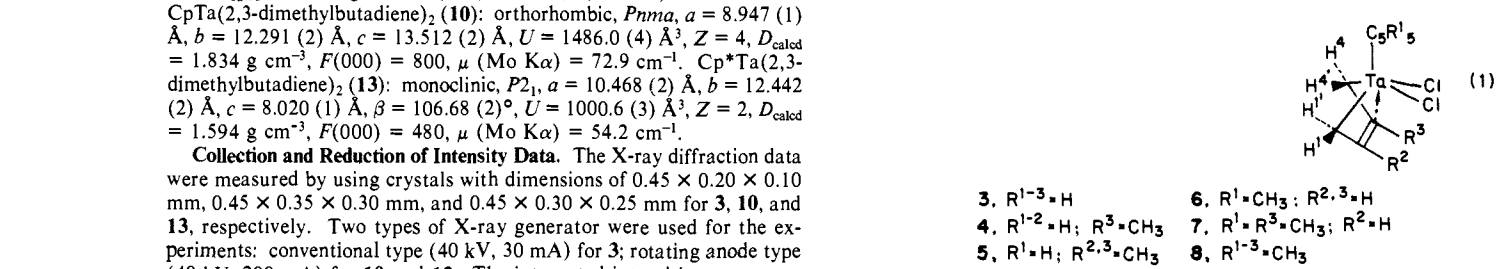

3, R^{1-3} = H
4, R^{1-2} = H; R^3 = CH_3
5, R^1 = H; $R^{2,3}$ = CH_3
6, R^1 = CH_3; $R^{2,3}$ = H
7, R^1 = R^3 = CH_3; R^2 = H
8, R^{1-3} = CH_3

diyl)magnesium or its higher homologues $-[MgCH_2CR{=}CRCH_2-]_n$ (R = H, Me) to a THF solution of $CpTaCl_4$ led to the formation of $CpTaCl_2$(diene) in good yield. Purification of the product by recrystallization from oxygen-free hexane and/or sublimation in vacuo (10^{-4} torr) gave $CpTaCl_2$(butadiene) (**3**), $CpTaCl_2$(isoprene) (**4**), or $CpTaCl_2$(2,3-dimethylbutadiene) (**5**) as diamagnetic purple crystals. Their structures were determined by spectral (NMR, MS, UV) and elemental analyses and finally by X-ray analysis. The basis for the formulation of the complexes shown in eq 1 will be described later in this paper.

Analogous complexes bearing a bulkier ligand, Cp^*TaCl_2(butadiene) (**6**), Cp^*TaCl_2(isoprene) (**7**), and Cp^*TaCl_2(2,3-dimethylbutadiene) (**8**), were prepared in a similar manner. Though preparation and NMR studies on two related tantalum–butadiene complexes, $TaCl(PMe_3)_2$(butadiene)(ethylene)[17] and $Cp^*TaCH_2CH_2CH_2CH_2$(butadiene),[18] have been reported briefly, the present method is advantageous for the systematic synthesis of alkylated derivatives. The previously reported procedure is effective only for the preparation of butadiene complexes since their diene units are constructed by dimerization of ethylene followed by double β-elimination.

(b) Tantalum–Bis(diene) Complexes. $CpTa(diene)_2$ and $Cp^*Ta(diene)_2$ containing two diene ligands in a molecule were prepared in good yields by treating $CpTaCl_4$ or Cp^*TaCl_4 with

(11) North, A. C. T.; Phillips, D. C.; Matthews, F. S. *Acta Crystallogr.* **1968**, *A24*, 351.

(12) Crystallographic data of $(\eta$-$C_5Me_5)Ta$(2,3-dimethylbutadiene)$_2$ at −60 °C: a = 10.451 (2) Å, b = 12.371 (2) Å, c = 8.004 (1) Å, β = 106.72 (1)°, U = 991.0 (3) Å^3, D_{calcd} = 1.610 g cm^{-3}.

(13) (a) Hoffmann, R. *J. Chem. Phys.* **1963**, *39*, 1397. (b) Ammeter, J. H.; Bürgi, H. B.; Thibeault, J. C.; Hoffmann, R. *J. Am. Chem. Soc.* **1978**, *100*, 3686.

(14) Kubáček, P.; Hoffmann, R., Havlas, Z. *Organometallics* **1982**, *1*, 180.

(15) Basch, H.; Gray, H. B. *Theor. Chim. Acta* **1966**, *4*, 367.

(16) Summerville, R. H.; Hoffmann, R. *J. Am. Chem. Soc.* **1976**, *98*, 7240.

(17) Fellmann, J. D.; Rupprecht, G. A.; Schrock, R. R. *J. Am. Chem. Soc.* **1979**, *101*, 5099.

(18) Mayer, J. M.; Bercaw, J. E. *J. Am. Chem. Soc.* **1982**, *104*, 2157.

Table I. ^{1}H NMR Parameters for $(\eta\text{-}C_5R_5)TaCl_2(diene)$ (R = H, CH_3)[a]

complexes (R)	chemical shift values, ppm			coupling constant, Hz						
	ν_1 (ν_4)	$\nu_{1'}$ ($\nu_{4'}$)	ν_2 (ν_3)	$J_{1,1'}$ ($J_{4,4'}$)	$J_{1,2}$ ($J_{3,4}$)	$J_{1',2}$	$J_{2,3}$	$J_{1,4}$	$J_{1,4'}$	$J_{2,4}$
3 (H)	0.96	0.19	7.03	−6.5	7.5	6.5	6.5	0.5	0.8	−2.0
4 (H)	1.08 (H^1)	0.39 ($H^{1'}$)	6.64	−7.3	7.3	6.3		1.5	1.5	−2.0
	1.10 (H^4)	0.14 ($H^{4'}$)								
5 (H)	0.69	0.40		−6.0				1.0	1.2	
6 (CH_3)	0.85	−0.09	7.09	−7.0	8.5	6.0	6.0	1.0	1.2	−2.2
7 (CH_3)	0.98 (H^1)	−0.02 (H^4)	6.67	−7.5	7.2	6.1		1.0	1.0	−1.0
	0.98 (H^4)	−0.12 (H^4)								
8 (CH_3)	0.54	0.02		−7.2				0.1	1.2	
$Zr(C_4H_6)$[b] (s-cis)	3.45	−0.69	4.78	−10.0	9.5	10.5	8.0	0.2	0.2	−1.5
$Zr(C_4H_6)$[c] (s-trans)	3.22	1.22	2.90	−4.0	7.1	16.4	15.0	0.5	0.02	−0.5
$Fe(C_4H_6)$[d]	2.32	0.49	5.27	−2.4	6.9	9.3	4.7	0.1	0.1	1.1

[a] Parameters were determined by computer simulation of the spectrum (100 MHz) measured in C_6D_6 at 30 °C. Chemical shift values are calibrated by using C_6H_6 as an internal standard, assumed to be 7.20 ppm. [b] Data for $Cp_2Zr(s\text{-}cis\text{-}C_4H_6)$.[5] [c] Data for $Cp_2Zr(s\text{-}trans\text{-}C_4H_6)$.[5] [d] Data for $Fe(CO)_3(C_4H_6)$.[19]

2 equiv of (2-butene-1,4-diyl)magnesium or its higher homologues in tetrahydrofuran (eq 2). Recrystallization from hexane at −20

$$(\eta\text{-}C_5R'_5)TaCl_4 + \text{-[-}MgCH_2CR^2{=}CR^3CH_2\text{-]}_n\text{-} \longrightarrow \quad (2)$$

R^1, H: CH_3

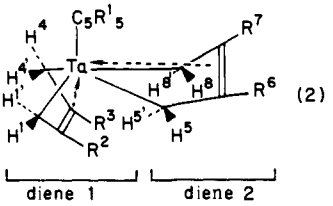

9, $R^{1\text{-}3}{=}R^{6,7}{=}H$
10, $R^1{=}H$; $R^{2,3}{=}R^{6,7}{=}CH_3$
11, $R^1{=}CH_3$; $R^{2,3}{=}R^{6,7}{=}H$
12, $R^1{=}R^3{=}R^7{=}CH_3$; $R^2{=}R^6{=}H$
13, $R^{1\text{-}3}{=}R^{6,7}{=}CH_3$

°C followed by sublimation gave complexes **9–13** as diamagnetic pale yellow crystals.

Under argon the tantalum–diene complexes **3–13** are thermally stable indefinitely, but in air complexes **9–10** decomposed in a few minutes and complexes **3–8** and **11–13** in several hours. All the complexes are immediately decomposed in protic solvents. Mass spectral analysis confirmed that complexes **3–13** exist in the monomeric form. Electron impact on **3–8** resulted in the release of coordinated diene generating a low-valent metal species, $CpTaCl_2$ or Cp^*TaCl_2, in good yield but the complexes **9–13** gave complicated metal species as confirmed by the mass spectrum.

Mode of Diene Coordination in Tantalum–Mono(diene) Complexes. (a) NMR studies. The remarkable features in structure and bonding of $LTaCl_2(diene)$ (**3–8**) were revealed by ^{1}H NMR spectroscopy. The static NMR parameters extracted from the computer simulation are given in Table I. As a typical example, the spectrum of **3** is shown in Figure 1. The spectral pattern for **3** and **6** differs significantly in two important aspects from that of conventional η^4-1,3-diene–metal complexes. Especially noteworthy is the small coupling constant of vicinal $J_{1',2}$ (6.0–6.5 Hz) compared to vicinal $J_{1,2}$ (7.2–8.5 Hz) as shown in Table I where $H^1(H^4)$ denotes the syn proton and $H^{1'}(H^{4'})$ the anti with respect to $H^2(H^3)$. The relative values of their spin–spin coupling constants do not conform to the general trend that $J_{1,2} < J_{1',2}$. This conflict may be rationalized by considering the bent metallacyclopent-3-ene structure that emphasizes the σ-bonding at the terminal carbon and the π-bonding at the inner carbon atoms of the diene unit (see eq 1). The magnitude of $J_{1',2}$ would decrease as the terminal proton ($H_{1'}$) bends out of the C(1)–C(4) plane. The enhanced sp^3 character of the terminal carbon was confirmed by relatively large absolute values of geminal coupling constant and by the chemical shift values. The difference in chemical shift between syn- and anti-protons is significantly smaller than that

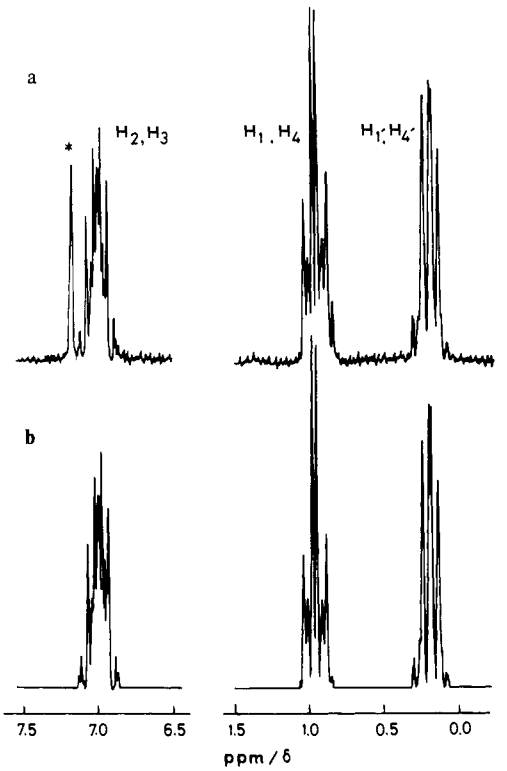

Figure 1. ^{1}H NMR spectrum (100 MHz) of $(\eta\text{-}C_5H_5)TaCl_2(C_4H_6)$ (**3**) in C_6D_6 at 30 °C: (a) observed and (b) simulated. The signal of Cp is omitted.

for $Fe(CO)_3(diene)$.[19] Reference can also be made to the ^{13}C NMR studies described later.

The other feature in the spectra of **3** and **6** is an unusually low-field shift of the olefinic protons (H^2 and H^3). The chemical shifts (ca. 7 ppm) for **3**, **6**, and the related complex $Cp^*\text{-}\overline{TaCH_2CH_2CH_2CH_2}(C_4H_6)$ (16 e^- configuration if dienes are assumed to be a 4 e^- ligand) are much larger than those (ca. 5.2–5.8 ppm) for group 8–10 metal–diene complexes as well as for Ta–bis(diene) complexes which possess the 18 e^- configuration. The chemical shift values of H^2 for **4** and **7** are also high. The combined effect of a large magnetic anisotropy and the absence of back donation may account for the strong deshielding of the $H^2(H^3)$ protons for **3**, **4**, 6, and **7**.

As a result, the structure of **3** may be expressed as the bent metallacyclopent-3-ene structure **14** or **15** rather than the conventional metal–η^4-1,3-diene structure **16** (supine) or **17** (prone)

(19) (a) Bachmann, K.; von Philipsborn, W. *Org. Magn. Reson.* **1976**, *8*, 648. (b) Ruh, S.; von Philipsborn, W. *J. Organomet. Chem.* **1977**, *127*, C59.

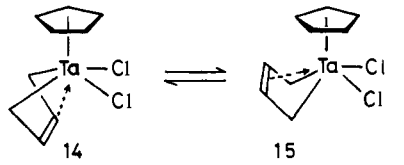

(3)

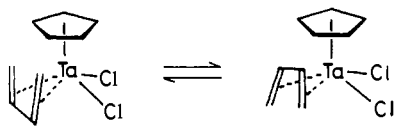

(4)

(naming, supine and prone, is employed for convenience of discussion on the geometry of Ta-bis(diene) complexes described later). If the Cp group is considered to occupy only one coordination site and the diene ligand to occupy two coordination sites via its terminal carbon atoms, the square-pyramidal geometry is most probable, since the pentacoordinated complexes of the type $CpTaL_4$[20] or $CpNbL_4$[21] generally assume the four-legged piano-stool geometry.

(b) X-ray Analysis of $CpTaCl_2$(butadiene) (3). The molecular structure of **3** was established by single-crystal X-ray diffraction. Different views of the molecule, along with the numbering scheme adopted, are displayed in Figure 2. A listing of the relevant bond distances and angles is given in Table II. The structure of **3** is best described as having the geometry **14**, where butadiene is bound to the metal in 1,4-fashion and the Cp ring is symmetrically pentahapto-bound with the Ta–C distances in a narrow range. The coordination sphere of the Ta atom resembles that found in a saturated metallacycle, $Cp^*TaCl_2(C_4H_8)$ (**18**), reported by Churchill.[23] However, the bond distances and angles for **3** significantly differ from those for **18** in the following aspects. (1)

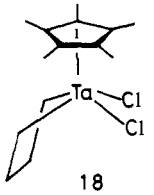

18

The C(2)–C(3) distance (1.375 Å) is shorter than the C(2)–C(3) bond distance of **18** reflecting the 2-butene-1,4-diyl structure. The distance is among the shortest C(2)–C(3) bond distances reported for metal–diene complexes and close to or even slightly shorter than those in Cp_2Zr(diene) complexes (1.391–1.398 Å)[7] and $Fe(CO)_4(C_4F_6)$ (1.38 Å).[24] (2) The C(1)–C(2) (1.458 Å) and C(3)–C(4) (1.453 Å) bond distances for **3** are shorter than that of the C(1)–C(2) single bond in **18** (1.552 Å) but nearly equal to those (1.451–1.474 Å) observed for Cp_2Zr(diene).[7] (3) Ta–C(2) (2.424 Å) and Ta–C(3) (2.410 Å) bond distances are much shorter than those (2.869 Å) in **18**, while Ta–C(1) (2.258 Å) and Ta–C(4) (2.257 Å) bonds are slightly longer than the Ta–C(1) and Ta–C(4) bonds (2.217 Å) in **18**. (4) The bent angle between the C(1)–C(2)–C(3)–C(4) and C(1)–Ta–C(4) planes (94.9°) is remarkably small compared with that (116.3°) for **18**. The value is intermediate between the angle for Cp_2Zr(diene) (112.0–123.4°) and that for the diene complexes of group 8–10 transition metals (<90°). (5) The C(1)–C(2)–C(3) (116.6°) and C(2)–C(3)–C(4) angles (117.3°) are larger than that in **18** (110.1°) but smaller than those (121.2–129.7°) for Cp_2Zr(diene) complexes. These

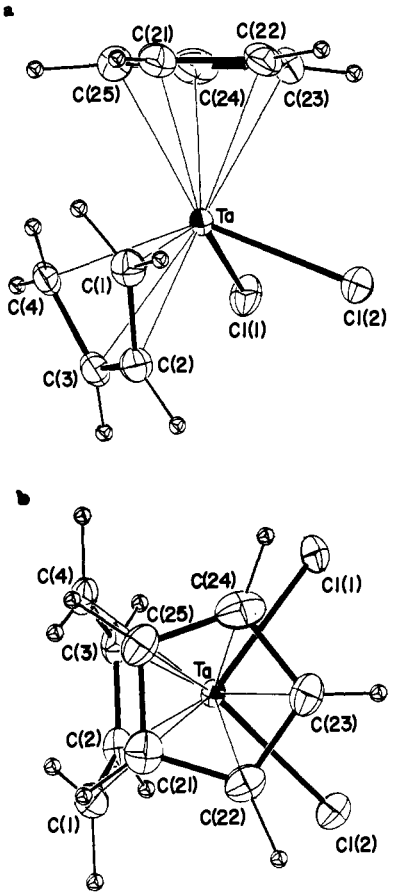

Figure 2. Molecular structure of $(\eta\text{-}C_5H_5)TaCl_2(C_4H_6)$ (**3**) drawn by ORTEP-II:[22] (a) the projection along the Cp plane and (b) the projection onto the Cp plane. Thermal ellipsoids for non-hydrogen atoms are given at the 20% probability level and the hydrogen atoms as spheres with an arbitrary temperature factor of 1.0 Å^2.

differences support the idea that a strong π-interaction exists between the metal and the unsaturated C(2)–C(3) bond in **3**.

Molecular Structure of Tantalum-Bis(diene) Complexes. (a) NMR studies. In general, the following three structures are to be considered for metal–bis(diene) complexes. Most of the bis(diene)metal complexes of the type $LM(diene)_2$ including $FeL(butadiene)_2$ (L = CO, PR_3),[25a,b] $Ru(CO)(diene)_2$,[25c] $RhCl(butadiene)_2$,[26] $IrCl(butadiene)_2$,[27] and $MnL(butadiene)_2$ (L = PR_3, CO)[28] assume the structure **19** with nearly C_{2v} symmetry where

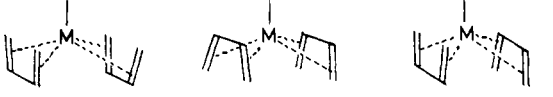

two diene ligands lie supine if the Cp ring looks upward. The complexes with structure **20** or **21** where two dienes lie in prone–prone or supine–prone have not been reported so far (see ref 29 for nomenclature). The NMR studies on the complexes

(20) (a) Werner, R. P. M.; Filbey, A. H.; Manastyrsky, S. A. *Inorg. Chem.* **1964**, *3*, 298. (b) Wood, C. D.; Schrock, R. R. *J. Am. Chem. Soc.* **1979**, *101*, 5421.

(21) Guggolz, E.; Ziegler, M. L.; Biersack, H.; Hermann, W. A. *J. Organomet. Chem.* **1980**, *194*, 317.

(22) Johnson, C. K. ORTEP-II, Report ORNL-5138, Oak Ridge National Laboratory, Oak Ridge, TN, 1974.

(23) (a) Churchill, M. R.; Youngs, W. J. *J. Am. Chem. Soc.* **1979**, *101*, 6462. (b) Churchill, M. R.; Youngs, W. J. *Inorg. Chem.* **1980**, *19*, 3106.

(24) Hitchcock, P. B.; Mason, R. *J. Chem. Soc., Chem. Commun.* **1967**, 242.

(25) (a) Whiting, D. A. *Cryst. Struct. Commun.* **1972**, *1*, 379. (b) Fischler, I.; Koerner von Gustorf, E. A. *Z. Naturforsch., B* **1975**, 30b, 291. (c) Noda, I.; Yasuda, H.; Nakamura, A. *Organometallics* **1983**, *2*, 1207.

(26) (a) Porri, L.; Lionetti, A.; Allegra, G.; Immirzi, A. *J. Chem. Soc., Chem. Commun.* **1965**, 336. (b) Immirzi, A.; Allegra, G. *Acta Crystallogr., Sect. B* **1969**, *B25*, 120.

(27) van Soest, T. C.; van der Ent, A.; Royers, E. C. *Cryst. Struct. Commun.* **1973**, *3*, 527.

(28) (a) Huttner, G.; Neugebauer, D.; Razavi, A.; *Angew. Chem.* **1975**, *87*, 353. (b) Harlow, R. L.; Krusic, P. J.; McKinney, R. J.; Wreford, S. S. *Organometallics* **1982**, *1*, 1506.

(29) The terms prone and supine were used in this paper to describe the orientation of the coordinated dienes. The conventional naming, exo and endo, does not seem suitable for the present unique stereochemistry.

Table II. Interatomic Bond Distances (Å) and Angles (Deg) for $CpTaCl_2$(butadiene) (**3**) and Estimated Standard Deviations in Parentheses

atoms	distance	atoms	distance
Ta–Cl(1)	2.423 (3)	C(1)–C(2)	1.458 (16)
Ta–Cl(2)	2.405 (3)	C(2)–C(3)	1.375 (16)
Ta–C(1)	2.258 (12)	C(3)–C(4)	1.453 (16)
Ta–C(2)	2.424 (11)	C(21)–C(22)	1.405 (17)
Ta–C(3)	2.410 (12)	C(21)–C(25)	1.410 (17)
Ta–C(4)	2.257 (11)	C(22)–C(23)	1.420 (17)
Ta–C(21)	2.393 (13)	C(23)–C(24)	1.423 (19)
Ta–C(22)	2.421 (12)	C(24)–C(25)	1.406 (19)
Ta–C(23)	2.412 (12)	mean[d] C–H	1.03 (13) (0.89–1.10)
Ta–C(24)	2.413 (15)		
Ta–C(25)	2.405 (12)		
Ta–CCP[a]	2.088		
Ta–M1[b]	1.811		
Ta–M2[c]	1.714		

atoms	angle	atoms	angle
Cl(1)–Ta–Cl(2)	89.5 (1)	C(1)–C(2)–C(3)	116.6 (10)
C(1)–Ta–C(4)	73.3 (4)	C(2)–C(3)–C(4)	117.3 (10)
C(2)–C(1)–Ta	78.2 (7)	C(22)–C(21)–C(25)	108.9 (11)
C(3)–C(4)–Ta	77.7 (7)	C(21)–C(22)–C(23)	108.1 (10)
CCP–Ta–M1	113.4	C(22)–C(23)–C(24)	106.7 (11)
CCP–Ta–M2	120.1	C(23)–C(24)–C(25)	109.0 (12)
M1–Ta–M2	126.5	C(24)–C(25)–C(21)	107.2 (11)
		mean[d] C–C–H(diene)	121 (7) (115–125)
		C–C–H(Cp)	126 (7) (121–131)
		H–C–H	119 (11) (114–124)

[a] CCP: centroid of cyclopentadienyl ligand (Cp). [b] M1: midpoint of C(1) and C(4). [c] M2: midpoint of Cl(1) and Cl(2). [d] Only mean values of bond distances and angles involving hydrogen atoms are listed. Esd's are in the first set of parentheses and ranges in the second.

9–13 clearly indicate that these complexes assume structure **21**, the first example of this type of complexation where two diene entities are magnetically inequivalent. The validity of this assignment was eventually justified by X-ray analyses of **10** and **13** and also by MO calculations as described later.

NMR parameters for the tantalum–bis(diene) complexes are given in Table III. The spectral pattern of $CpTa(butadiene)_2$ (**9**) at 20 °C is discussed here as a typical example. One of the butadiene ligands (diene-1 lying supine) gives a set of three resonances at 2.49 (H^1 and H^4, syn protons), 0.30 ($H^{1'}$ and $H^{4'}$, anti protons), and 4.93 ppm (H^2 and H^3, inner protons). The NMR parameters for the other butadiene ligand (diene-2) differ from that for the diene-1 in the following aspects. The chemical shift value of $H^6(H^7)$ in diene-2 is smaller than that of $H^2(H^3)$ in diene-1. From $(\nu_1 + \nu_{1'})/2 > (\nu_5 + \nu_{5'})/2$, it follows that the diene-2 ligand is highly shielded by the adjacent Cp ring when compared with the diene-1. The magnitude of $J_{1,2}(J_{3,4})$ for diene-1 is slightly larger than that of $J_{1',2}(J_{3,4'})$ in accord with the relationship observed in the spectra of mono(diene) complexes **3**, **4**, **6**, and **7**, while the magnitude of $J_{5,6}(J_{7,8})$ for diene-2 is smaller than that of $J_{5',6}(J_{7,8'})$ (the data for H^7 and H^8 are omitted in Table III since they are identical with those for H^6 and H^5). The complexes **11** and **12** showed a similar trend (see Experimental Section, simulation not applied). The validity of the above noted assignment was justified by comparison with the assignment resulting from variable-temperature NMR studies on **13** coupled with its X-ray analysis and also by the X-ray work on a mixed-diene complex (**22**), the preparation of which will be given later in this text.

The chemical shifts of $H^2(H^3)$ and $H^6(H^7)$ in complex **9** compare closely to those of $Fe(CO)_3(C_4H_6)$ and $FeL(C_4H_6)_2$ (see Tables I and III) rather than those for $CpTaCl_2(C_4H_6)$ (**3**), but the absolute values of $J_{1,1'}$ and $J_{5,5'}$ differ significantly from those for Fe–diene complexes since the Ta–C_4H_6 complex possesses the strong 1,4-σ-bonding character. A detailed comparison of the NMR data for the diene-2 unit in complex **9** with those for the C_4H_6 ligand in complexes **3** and **6** suggests an appreciable contribution of η^4-1,3-diene character for the diene-2 moiety; i.e., the chemical shift values and the relative values of the coupling constants ($J_{5,6'} > J_{5,6}$) resemble to some extent those for Fe–diene complexes.

Though the group 4 metal–diene complexes occasionally favor the *s-trans*-diene coordination, such type of bonding was not found in the present complexes.

(b) ^{13}C NMR Spectra. The ^{13}C NMR chemical shifts and the

Table III. ^1H NMR Parameters for $(\eta\text{-}C_5R_5)Ta(diene)_2$ (R = H, CH_3) and Related Complexes[a]

complexes (R)	diene-1 diene-2	chemical shift values, ppm $\nu_1(\nu_4)$ $\nu_{1'}(\nu_{4'})$ $\nu_2(\nu_3)$ $\nu_5(\nu_8)$ $\nu_{5'}(\nu_{8'})$ $\nu_6(\nu_7)$			coupling constant, Hz $J_{1,1'}$ $J_{1,2}$ $J_{1',2}$ $J_{2,3}$ $J_{5,5'}$ $J_{5,6}$ $J_{5',6}$ $J_{6,7}$			
9 (H)	C_4H_6	2.49	0.30	4.93	−6.2	8.2	6.5	7.0
	C_4H_6	1.84	0.45	4.40	−5.8	9.5	11.0	8.5
10 (H)	C_6H_{10}	1.78	0.05		−8.0			
	C_6H_{10}	1.45	−0.28		−8.0			
13 (CH_3)	C_6H_{10}	0.69	−0.63		−7.5			
[50 °C]	C_6H_{10}	0.89						
13 (CH_3)	C_6H_{10}	1.14	−0.36		−7.5			
[−70 °C]	C_6H_{10}	1.18	−0.76		−11.1			
22 (CH_3)	C_6H_{10}	1.70	−0.08		−7.5			
	C_4H_6	1.58	0.04	4.34	−5.8	9.5	11.0	8.5
$Fe(C_4H_6)_2PPh_3$[b]		1.26	−1.38	4.57	1.2	6.5	8.9	?

[a] Data were collected at 100 MHz in C_6D_6 at 30 °C except for **13** and the parameters were determined by computer simulation. [b] Data reported by Fischler.[26b] $J_{1,3}$ for **9**, 0.8 Hz; $J_{5,7}$ for **9** and **22**, 1.5 Hz; $J_{1,3}$, and $J_{5,7'}$ for **9** and **22**, −1.5 Hz.

Table IV. ^{13}C NMR Chemical Shift Values (ppm) and ^{13}C–^1H Coupling Constants (Parentheses, Hz) for Tantalum–Bis(diene) and Related Complexes[a]

complexes	C-1 (C-4)	C-2 (C-3)	C-5 (C-8)	C-6 (C-7)
9	35.9 (t, 150)	113.8 (d, 156)	37.2 (t, 148)	103.7 (d, 155)
10	43.9 (t, 138)	117.2 (s)	43.9 (t, 140)	114.7 (s)
11	38.8 (t, 146)	114.9 (d, 159)	42.3 (t, 147)	104.8 (d, 160)
13	53.2 (t, 134)	123.4 (s)	57.6 (t, 140)	119.0 (s)
22	47.6 (t, 141)	116.4 (s)	40.4 (t, 146)	105.4 (t, 156)
3	62.4 (t, 146)	126.1 (d, 169)		
$Zr(C_4H_6)$[b]	48.4 (t, 145)	110.9 (d, 154)		
$Zr(C_6H_{10})$[c]	46.7 (t, 143)	122.2 (s)		
$Hf(C_6H_{10})$[d]	52.1 (t, 132)	122.1 (s)		

[a] In ppm down field from the external Me_4Si. Data were collected in C_6D_6 at 30 °C. [b] Data for Cp_2Zr(*s-cis*-C_4H_6).[2e] [c] Data for Cp_2Zr(*s-cis*-2,3-dimethylbutadiene).[2e] [d] Data for Cp_2Hf(*s-cis*-2,3-dimethylbutadiene).[5b]

Table V. Interatomic Bond Distances (Å) and Angles (Deg) for CpTa(2,3-dimethylbutadiene)$_2$ (**10**) and Estimated Standard Deviations in Parentheses

atoms	distance	atoms	distance
Ta–C(1)	2.261 (8)	C(1)–C(2)	1.469 (11)
Ta–C(2)	2.522 (7)	C(2)–C(2′)	1.352 (14)
Ta–C(11)	2.292 (7)	C(2)–C(5)	1.525 (12)
Ta–C(12)	2.473 (8)	C(11)–C(12)	1.475 (11)
Ta–C(21)	2.482 (11)	C(12)–C(12′)	1.343 (15)
Ta–C(22)	2.411 (13)	C(12)–C(15)	1.544 (13)
Ta–C(23)	2.419 (16)	C(21)–C(22)	1.444 (16)
Ta–CCP[a]	2.119	C(21)–C(21′)	1.406 (21)
Ta–M1[b]	1.796	C(22)–C(23)	1.416 (20)
Ta–M2[c]	1.797	mean C–H	1.07 (12) (0.99–1.17)

atoms	angle	atoms	angle
C(1)–Ta–C(1′)	74.8 (3)	C(1)–C(2)–C(2′)	118.4 (7)
C(11)–Ta–C(11′)	76.7 (3)	C(1)–C(2)–C(5)	118.5 (7)
C(2)–C(1)–Ta	82.1 (4)	C(5)–C(2)–C(2′)	123.1 (7)
C(12)–C(11)–Ta	78.8 (4)	C(11)–C(12)–C(12′)	120.6 (7)
CCP–Ta–M1	108.5	C(11)–C(12)–C(15)	115.9 (7)
CCP–Ta–M2	137.2	C(15)–C(12)–C(12′)	123.3 (7)
M1–Ta–M2	114.3	C(22)–C(21)–C(21′)	108.1 (10)
		C(21)–C(22)–C(23)	107.4 (11)
		C(22)–C(23)–C(22′)	108.8 (13)
		mean C–C–H(diene)	119 (6) (114–123)
		C–C–H(Cp)	126 (7) (121–131)
		H–C–H	120 (9) (118–122)

[a] CCP and mean are the same as those in Table II. [b] M1, midpoint of C(1) and C(1′). [c] M2, midpoint of C(11) and C(11′).

^{13}C–^{1}H coupling constants for Ta–bis(butadiene) (**9**, **11**), Ta–bis(2,3-dimethylbutadiene) (**10**, **13**), and the mixed-diene complex (**22**) are shown in Table IV. The ^{13}C–^{1}H coupling constants of terminal CH_2 for 2,3-dimethylbutadiene ligand in **10**, **13**, and **22** (134–141 Hz) are significantly smaller than those of conventional η^4-1,3-diene complexes (158–161 Hz), indicating that these carbon atoms have an enhanced sp^3 character. The $J_{1,1'}$($J_{5,5'}$) values given in Table III also support the above prediction.

The extent of sp^n hybridization for **10** and **13** was roughly calculated to be n = 2.6–2.7 using Newton's semiempirical equation.[30] The corresponding coupling constants for bis(butadiene) analogues (**9**, **11**) are slightly larger (146–150 Hz) and the sp^n hybridization is estimated to be on the order of n = 2.5. The increased sp^3 character of $C_1(C_4)$ atoms in **10** and **13** is attributable to the inductive effect of methyl substituents on C_2 and C_3 atoms and similar effect of substitution has been found in Cp_2M(*s-cis*-diene) (M; Zr, Hf).[5] In the case of Cp_2Hf(2,3-dimethylbutadiene), the n value increases up to 2.8 and the s-cis coordinated diene molecule is highly fluxional even at −70 °C.[2a,5] Thus we can conclude that the extent of sp^n hybridization for the $C_1(C_4)$ atoms in Ta–diene complexes is intermediate between those of group 4 metal–diene and group 8–10 metal–diene complexes.

(c) X-ray Analysis of Cp_2Ta(2,3-dimethylbutadiene)$_2$ (10). The molecular structure of **10** deduced from X-ray analysis is shown in Figure 3. Selected bond distances and angles are summarized in Table V. The tantalum atom may be described as having a pseudo-square-pyramidal geometry if the Cp group is considered to occupy only one coordination site and each of the 2,3-dimethylbutadiene ligands is assumed to bind via the two terminal carbon atoms. The most noteworthy feature is the unique orientation of the two diene ligands that comprises the supine–prone structure. Such type of coordination has not yet been reported. The plane of the diene-1 ligand composed of C(1), C(2), C(2′), and C(1′) is nearly perpendicular to the Cp ring, the dihedral angle being 81.5°, slightly larger than that in **3** (71.9°) but smaller than that in **18** (92.5°). On the other hand, the plane of diene-2 defined by C(11), C(12), C(12′), and C(11′) makes an acute angle (35.0°)

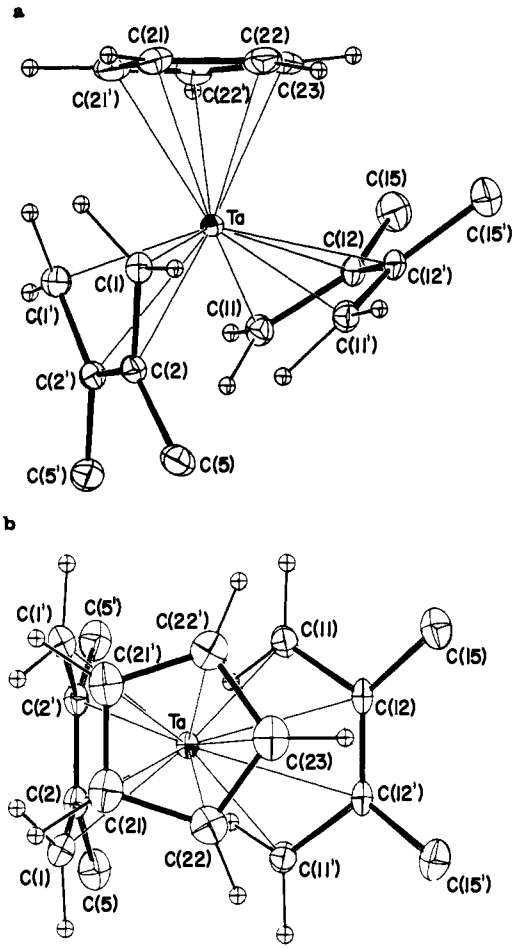

Figure 3. Molecular structure of (η-C_5H_5)Ta(C_6H_{10})$_2$ (**10**): (a) projected along the Cp plane and (b) projected onto the Cp plane. Drawing parameters are the same as those given in Figure 2.

with the Cp ring. The dihedral angle between the two diene planes is 63.6°. An examination of the bond lengths supports the view obtained from the NMR studies that the diene is bound in the bent 2-butene-1,4-diyl fashion rather than conventional η^4-1,3-diene coordination; i.e., both the C(2)–C(2′) (1.352 Å) and the C(12)–C(12′) (1.343 Å) bonds are shorter than the C(1)–C(2), C(1′)–C(2′), C(11)–C(12), or C(11′)–C(12′) bonds by ca. 0.11–0.13 Å. The dihedral angles for the tantalacyclopent-3-ene moieties containing diene-1 and diene-2 are 102.5° and 100.4°, respectively, 5.5–7.6° larger than that in **3**. The Ta–C(1) and Ta–C(11) distances (2.261 and 2.292 Å) are similar to those in $CpTaCl_2(C_4H_6)$ (**3**), while the Ta–C(2) (2.522 Å) and Ta–C(12) (2.473 Å) bonds are longer than those in **3**. Thus, the whole geometry of **10** is not superimposable to any of the geometry reported for L_nM(diene)$_2$ (M: Fe, Rh, Ir, Mn) of prone–prone orientation. The geometry is also different from the uniquely distorted octahedral structure reported for Hf(butadiene)$_2$(1,2-bis(dimethylphosphino)ethane) where two diene ligands are in a skewed position to each other.[31]

(d) Synthesis of Mixed Bis(diene)tantalum Complexes. The present method provides a novel route for preparation of mixed bis(diene)metal complexes where the metal is coordinated by two different diene ligands. The chemistry of mixed bis(diene)tantalum complexes will provide useful information for the understanding of subtle differences in bonding and reactivity existing between the two diene ligands. Thus, Cp*Ta(butadiene)(2,3-dimethylbutadiene) was prepared by treating a 2,3-dimethylbutadiene complex **8** with (2-butene-1,4-diyl)magnesium according to the eq 5. The reaction left the molecular arrangement of **8** intact and gave an isomerically pure product in which butadiene

(30) Newton, M. D.; Shulmann, T. M.; Manus, M. M. *J. Am. Chem. Soc.* **1974**, *96*, 17.

(31) Wreford, S. S.; Whitney, J. F. *Inorg. Chem.* **1981**, *20*, 3918.

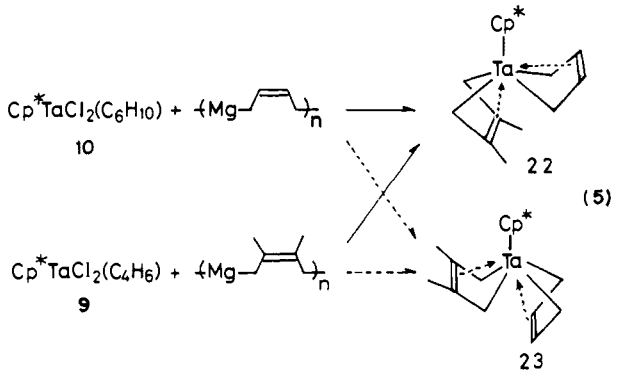

has the orientation shown as **22**. If the reaction involves the geometrical change leading to the complex **23**, the chemical shift of $H^{5'}$ of the 2,3-dimethylbutadiene ligand would have shifted to higher field as observed for diene-2 in complex **13**.

It should be noted that the reaction of Cp^*TaCl_2(butadiene) (**6**) with (2,3-dimethyl-2-butene-1,4-diyl)magnesium also gives rise to the formation of **22**, not the complex **23**, as revealed by NMR and preliminary X-ray work.[32] The geometrical change during this reaction may be rationalized by invoking an η-allylic metal species (**24**) involving an 1,4-σ-2,3-dimethylbutadiene ligand.

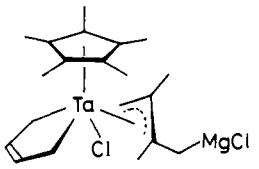

24

The steric repulsion between the methyl groups in Cp* and the diene ligand must be responsible for the geometrical change.

Dynamic Structure of $Cp^*Ta(diene)_2$. (a) NMR Studies. The complex **9** involving the C_5H_5 ligand shows a rigid metallacyclic structure even at high temperatures while the complex **13** with two bulky ligands, C_5Me_5 and 2,3-dimethylbutadiene, shows a unique fluxional behavior at 0–50 °C. When the complex **13** was cooled to −70 °C, the spectrum gives the limiting structure consisting of two AB quartets which are assignable to the respective terminal CH_2 protons. The chemical shift difference between H^1 and $H^{1'}$ at diene-1 is comparable to that between H^5 and $H^{5'}$, but the geminal coupling $J_{5,5'}$ is significantly larger than $J_{1,1'}$ which indicates that C_5 and C_8 atoms have an enhanced sp^3 character similar to that in Zr–diene complexes. This may be attributed to the large contribution of the 1,4-σ-planar metallacyclopent-3-ene structure enforced by the steric repulsion between methyl groups on Cp* and 2,3-dimethylbutadiene.

As temperature is increased from −70 to 50 °C, only the diene-2 unit of **13** becomes fluxional and the two doublets due to $H^5(H^8)$ and $H^{5'}(H^{8'})$ average to give a broad resonance at ca. 0.89 ppm, the spepectral pattern of the $H^1(H^4)$ and $H^{1'}(H^{4'})$ protons was largely unaffected. The flipping of the diene-2 unit may cause the fluxionalization through a 16 e^- intermediate. Similar configurational interconversion is reported also for $[CpMo(CO)_2$(diene)$]^+$.[33] Further heating of the sample to 100 °C resulted in the coalescence of the $H^1(H^4)$ and $H^{1'}(H^{4'})$ signals. However, the signals of the two diene units (H^1,$H^{1'}$, and H^5,$H^{5'}$) did not average (through 14 e^- intermediate) even at 135 °C where thermal decomposition begins to give a polymeric product. The addition of electron donors such as $P(C_2H_5)_3$ or pyridine did not bring about an acceleration of the fluxionality; i.e., no significant change in the spectral pattern was observed in the variable-temperature NMR spectrum which indicates that the coordination of these donors is not so strong as to cleave the π-bonding between the Ta and $C_2(C_3)$ atom. The thermal stability of **13** is much higher than that of $CpCl_2TaCH_2CMeCMeCH_2$ which decomposes at 25 °C to give coupling products of alkenes.[34]

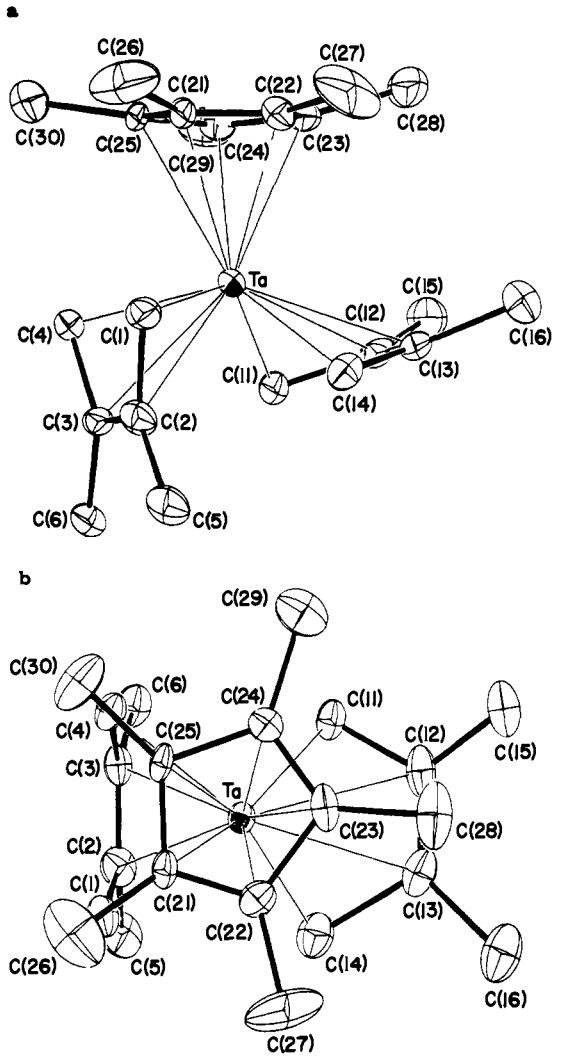

Figure 4. Molecular structure of $(\eta\text{-}C_5Me_5)Ta(C_6H_{10})_2$ (**13**) at 20 °C: (a) the projection along the Cp* plane and (b) the projection onto the Cp* plane. The drawing parameters follow those given in Figure 2.

(b) X-ray Analysis of $Cp^*Ta(2,3\text{-dimethylbutadiene})_2$ (13). The X-ray structure of **13** is shown in Figure 4. The important bond distances and angles are shown in Table VI. The geometrical situation of the two diene ligands surrounding the Ta atom is essentially the same as that in complex **10** except for the following. The plane of the diene-2 composed of the C(11)–C(14) atoms is nearly parallel to the Cp plane, the dihedral angle being 18.5°. The significantly small dihedral angle compared with that of **10** may be attributed to the nonbonded interatomic repulsions between the methyls attached to the Cp and the diene-2. The interatomic distance for C(15)–C(28) and C(16)–C(28) are 3.38 and 3.43 Å, respectively. So far such a planar metal–diene skeleton has only been reported for the metallacyclic structure of $Fe(CO)_4$-$(CF_2CF{=}CFCF_2)$ where the π-interaction between Fe and the C(2)–C(3) double bond is absent.[24] The dihedral angle between the Cp and diene-1 planes (83.5°) is comparable to that for **10**. As a consequence, the dihedral angle between the two diene planes becomes larger (78.6°) by 15° than that observed for **10**.

The structural parameters are of limited accuracy due to the rather big thermal vibrations even at −60 °C. The comparison of the X-ray data obtained at 20 °C with those at −60 °C revealed that the thermal motion of diene-2 fragment is more temperature

(32) Crystallographic data of $(\eta\text{-}C_5Me_5)Ta(C_4H_6)(C_6H_{10})$: F.W. = 452.4, orthorhombic, $Pca2_1$, 20 °C, a = 15.352 (2) Å, b = 8.259 (1) Å, c = 14.168 (3) Å, Z = 4, D_c = 1.672 g cm^{-3}, $F(000)$ = 896, μ (Mo Kα) = 91.7 cm^{-1}.

(33) Faller, J. W.; Rosan, A. M. *J. Am. Chem. Soc.* **1977**, *99*, 4859.

(34) McLain, S. L.; Sancho, J.; Schrock, R. R. *J. Am. Chem. Soc.* **1980**, *102*, 5610.

Table VI. Interatomic Bond Distances (Å) and Angles (Deg) for Cp*Ta(2,3-dimethylbutadiene)$_2$ (**13**) at 20 °C (Estimated Standard Deviations in Parentheses)

atoms	distance	atoms	distance
Ta-C(1)	2.29 (2)	C(1)-C(2)	1.52 (4)
Ta-C(2)	2.53 (4)	C(2)-C(3)	1.34 (4)
Ta-C(3)	2.55 (2)	C(3)-C(4)	1.48 (2)
Ta-C(4)	2.30 (1)	C(2)-C(5)	1.47 (4)
Ta-C(11)	2.20 (1)	C(3)-C(6)	1.50 (3)
Ta-C(12)	2.61 (3)	C(11)-C(12)	1.45 (3)
Ta-C(13)	2.60 (2)	C(12)-C(13)	1.33 (4)
Ta-C(14)	2.19 (2)	C(13)-C(14)	1.66 (3)
Ta-C(21)	2.52 (2)	C(12)-C(15)	1.47 (4)
Ta-C(22)	2.46 (1)	C(13)-C(16)	1.61 (3)
Ta-C(23)	2.47 (2)	C(21)-C(22)	1.29 (2)
Ta-C(24)	2.47 (1)	C(n21)-C(25)	1.40 (2)
Ta-C(25)	2.55 (2)	C(22)-C(23)	1.49 (2)
Ta-CCP[a]	2.19	C(23)-C(24)	1.34 (2)
Ta-M1[a]	1.86	C(24)-C(25)	1.47 (2)
Ta-M2[b]	1.67		

atoms	angle	atoms	angle
C(1)-Ta-C(4)	71.7 (5)	C(2)-C(3)-C(6)	122 (2)
C(11)-Ta-C(14)	80.7 (6)	C(4)-C(3)-C(6)	120 (2)
C(2)-C(1)-Ta	81 (2)	C(11)-C(12)-C(13)	118 (2)
C(3)-C(4)-Ta	82 (1)	C(11)-C(12)-C(15)	117 (2)
C(12)-C(11)-Ta	89 (1)	C(13)-C(12)-C(15)	124 (2)
C(13)-C(14)-Ta	84 (1)	C(12)-C(13)-C(14)	120 (2)
CCP-Ta-M1[a]	103.1	C(12)-C(13)-C(16)	131 (2)
CCP-Ta-M2[b]	142.2	C(14)-C(13)-C(16)	109 (2)
M1-Ta-M2	114.6	C(22)-C(21)-C(25)	110 (2)
C(1)-C(2)-C(3)	115 (3)	C(21)-C(22)-C(23)	109 (1)
C(1)-C(2)-C(5)	118 (3)	C(22)-C(23)-C(24)	108 (1)
C(3)-C(2)-C(5)	127 (3)	C(23)-C(24)-C(25)	106 (1)
C(2)-C(3)-C(4)	118 (2)	C(21)-C(25)-C(24)	108 (1)

[a] CCP and M1 are the same as those in Table II. [b] M2, midpoint of C(11) and C(14).

dependent than that of the diene-1 (the X-ray parameters are given as supplementary material). This result agrees with the NMR prediction that the diene-2 ligand is far more fluxional than the diene-1 fragment at room temperature. The positional ambiguity present in the analysis of **13** hampers a detailed structural comparison between **13** and **3** or **10**. The methyl groups attached to the Cp ring bend out from the Cp plane and the tilt angle (average 9.4°) is close to those for ketone adducts Cp*$_2$Zr($C_{11}H_{22}O$) (average 10.2°) and Cp*$_2$Zr($C_{12}H_{22}O$) (average 9.8°).[2e]

Remarkable Features in the Structures of Tantalum–Diene Complexes. This section describes the general structural feature of tantalum–diene complexes in comparison with the conventional metal–diene complexes. Among the various metal–diene complexes available in the Cambridge Crystallographic Database,[35] some of the molecular structures of acyclic diene complexes determined with sufficient accuracy were selected for our discussions. Cyclic and hindered diene complexes are excluded here. The correlation between the bent angle (θ) subtended by the C(1)–M–C(4) and C(1)–C(4) planes and the difference in M–C bond distances (Δd) defined by $\Delta d = [d(\text{M–C(1)}) + d(\text{M–C(4)})]/2 - [d(\text{M–C(2)}) + d(\text{M–C(3)})]/2$ are plotted in Figure 5. The bent angles for group 7 and 8–10 metal–diene complexes are in the narrow range 80–85° and the Δd ranges from 0 to 0.1 Å; i.e., the M–C(1) and M–C(4) bonds are nearly equal or slightly longer than the M–C(2) or M–C(3) bond. On the other hand, the bent angles in the group 4 and 5 metal complexes are larger than 90° and vary over a wide range, 95–120°, with a corresponding change in Δd of −0.4 to 0.0 Å. Thus the bent angles increase with decreasing Δd. The observed structural parameters for the group 4 and 5 metal complexes resemble those found for a magnesium–diene adduct, Mg(PhCHCH=CHCHPh)(THF)$_3$,[36] rather

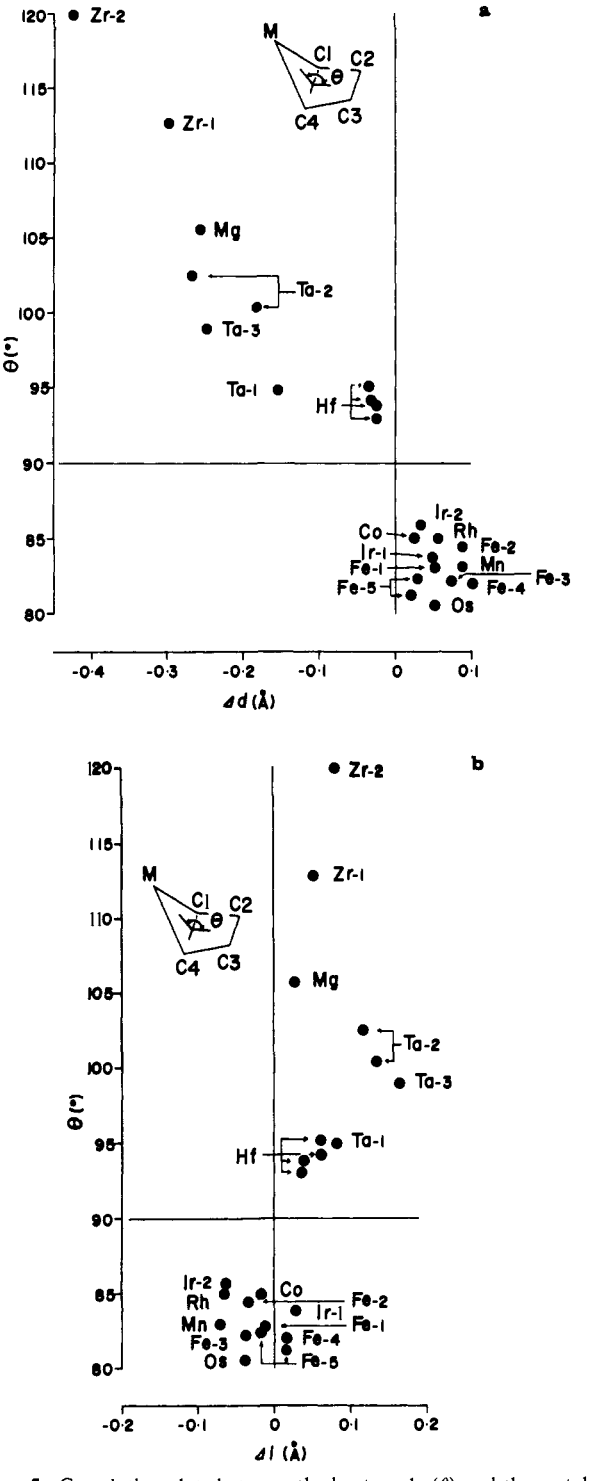

Figure 5. Correlation plots between the bent angle (θ) and the metal–carbon distance (d) or the carbon–carbon bond length (l) in the metal–diene complexes. (a) θ vs. $\Delta d = [d(\text{M–C1}) + d(\text{M–C4})]/2 - [d(\text{M–C2}) + d(\text{M–C3})]/2$. (b) θ vs. $\Delta l = [l(\text{C1–C2}) + l(\text{C3–C4})]/2 - l(\text{C2–C3})$. BD, 23DMBD, 23DPBD, and 14DPBD are abbreviations for butadiene, 2,3-dimethylbutadiene, 2,3-diphenylbutadiene, and 1,4-diphenylbutadiene, respectively. Mg, Mg(14DPBD)(THF)$_3$;[36] Zr-1, Cp$_2$Zr(23DMBD);[7a] Zr-2, Cp$_2$Zr(23DPBD);[7b] Hf, Hf(BD)$_2$(dmpe);[31] Ta-1, CpTaCl$_2$ (BD); Ta-2, CpTa(23DMBD)$_2$; Ta-3, Cp*Ta(23DMBD)$_2$; Mn, Mn(CO)(BD)$_2$;[28] Fe-1, Fe(CO)(23DMBD) [glyoxal-bis(isopropyl imine)];[37] Fe-2, Fe(CO)(BD)(COT);[38] Fe-3, Fe(CO)(BD)$_2$;[25] Fe-4, Fe(14DPBD)(CO)$_3$(14DPBD);[39] Fe-5, Fe(14DPBD)(CO)$_3$;[40] Os, Os$_3$(CO)$_{10}$(BD);[41] Co, [Co(23DMBD)(CO)$_2$]$_2$;[42] Rh, Rh(BD)$_2$Cl;[26] Ir-1, Ir(BD)H[P(C$_3$H$_7$)$_3$]$_2$;[43] Ir-2, Ir(BD)$_2$Cl.[27]

than those for the group 7 and 8–10 metal complexes.

At a rough estimate, a linear correlation is also observed between the bent angle and the difference in bond lengths defined

(35) "Cambridge Crystallographic Database User Manual", Crystallographic Data Center, University Chemical Laboratory, Cambridge, U.K., 1978.

(36) Kai, Y.; Kanehisa, N.; Miki, K.; Kasai, N.; Mashima, K.; Yasuda, H.; Nakamura, A. *Chem. Lett.* **1982**, 1277.

by $\Delta l = [l(C(1)-C(2)) + l(C(3)-C(4))]/2 - l(C(2)-C(3))$ as shown in Figure 5b. The bent angle (θ) increases with an increase of Δl. Thus the Δl for group 7 and 8–10 metal–diene complexes varies from −0.1 to 0.0 Å while the Δl for Mg–, Zr–, Hf–, and Ta–diene complexes ranges from 0.0 to 0.2 Å. The points for tantalum complexes (Ta-2, Ta-3) deviate slightly from the straight line even when the positional ambiguity is considered.

A Molecular Orbital Analysis of the Structure

The major object in this portion of the study is to outline the nature of Ta–butadiene bonding and to find electronic factors which determine the observed orientational preference of 1,3-dienes in **3–13**. Molecular orbital calculations at the extended-Hückel level were performed on $CpTaCl_2(C_4H_6)$ and $CpTa(C_4H_6)_2$ by using the computational and geometrical parameters given in the Experimental Section.

First compare the total energies calculated for the two orientations, supine (**25**) and prone (**26**), of the C_4H_6 group in

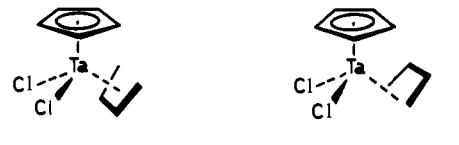

	L = 0.45 Å φ = 20°	L = 0.0 Å φ = 40°
ΔE (kcal/mol)	0.0	15.7
	supine	prone
	25	26

$CpTaCl_2(C_4H_6)$. Each geometry was roughly optimized by choosing two common geometrical variables L and φ as shown in **27**. L denotes the slide of butadiene upward, while φ defines

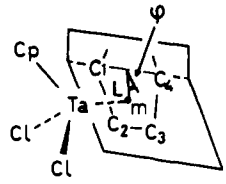

27

the swing motion of the inner carbon portion away from the metal. These parameters for geometrical optimization have also been used in our study on $Cp_2Zr(C_4H_6)$ and $Fe(CO)_3(C_4H_6)$.[44] For both conformations we fixed the Cp(centroid)–Ta–*m* angle at 120°. The relative total energies calculated for the two minima are given at the bottom of their structures. We calculate a strong preference of 15.7 kcal/mol for the supine isomer, which agrees nicely with our experimental finding and the structure of the analogous Nb complex, $CpNbCl_2[C_4H_2(CH_3)_4]$.[45]

To probe the reason behind this orientational preference, we analyze molecular orbitals of supine (**25**) and prone (**26**) structures of $CpTaCl_2(C_4H_6)$. In the optimized geometries, **25** and **26**, the butadiene group is deformed from its ideal planar structure, significantly so in the form **26**. The direct comparison between **25** and **26** thus would require us to consider the effect of different distortion upon the electronic structure. To avoid this complication, we here compare orbitals of the optimized supine form with its prone "rotamer" where L = 0.45 Å and φ = 20°. Note

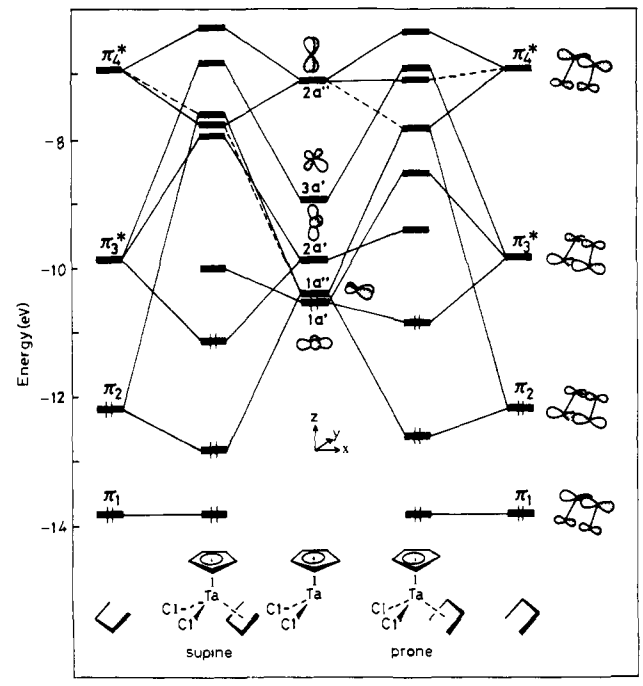

Figure 6. Orbital interaction digrams for the supine (L = 0.45 Å, φ = 20°) and prone (L = 0.45 Å, φ = 20°) rotamers of $CpTaCl_2(C_4H_6)$.

that the rotamer of **25** is 8.4 kcal/mol less stable than the optimized **26**.

Our approach in developing the molecular orbitals of $CpTaCl_2(C_4H_6)$ is to allow the important valence orbitals of the $CpTaCl_2$ fragment to interact with butadiene. Figure 6 provides such interaction diagrams for the supine (left) and prone (right) rotamers, where the orbitals of $CpTaCl_2$ are sketched in the middle. Since the $CpML_2$ fragment orbitals have been discussed in detail,[46] we will point out only the salient features of the $CpTaCl_2$ orbitals. The five valence orbitals consist primarily of Ta d orbitals, which are labeled either a′ or a″ depending on whether the orbital is symmetric or antisymmetric, respectively, to the *xz* mirror plane. Lying at lower energy, 1a′, 1a″, and 2a′, as well as somewhat higher lying 3a′, carry the coordinative unsaturation of the isolated $CpML_2$ fragment for a d^0 electron count. When any one of these orbitals is doubly occupied like the 1a′ of $CpTaCl_2$, then it behaves as a lone-pair orbital. The remaining 2a″ orbital lies high in energy due to the strong ligand field of Cp.

Interactions between the $CpTaCl_2$ orbitals and C_4H_6 π (or π^*) are not that simple because of the low molecular symmetry of C_s. In principle, π_1 and π_3^* are capable of overlapping with any of a′ orbitals, while π_2 and π_4^* find a symmetry match with a″ orbitals. For the supine form **25**, a significant interaction can be noticed to occur between π_2 and 1a″, another between π_3^* and a′. One may term them donation and back-donation types of interactions. The diagram for prone is similar to that for supine except that π_3^* interacts primarily with 1a′. The difference in total energies calculated for the two rotamers arises from the different magnitude of the donation and back-donation interactions. These are stronger in supine than in prone.

This trend can be traced to the calculated overlap integrals between the $CpTaCl_2$ fragment orbitals and butadiene π_2 and π_3^* as shown in Figure 7. The 2a′ orbital of $CpTaCl_2$ overlaps with π_3^* (supine) better than 1a′ does with π_3^* (prone). Also the 1a″–π_2 overlap integral is larger for the supine form. The different 1a″–π_2 overlaps derive from the specific shape of each orbital. In butadiene π_2, larger lobes are at the terminal carbon atoms. The $CpTaCl_2$ 1a″ tilts from the *xy* plane by 25° and interacts with these terminal lobes of π_2 more effectively in the structure **25** (supine). For prone (**26**), 1a″ is directed rather to the inner,

(37) Fruhauf, H.-W.; Wolmershauser, G. *Chem. Ber.* **1982**, *115*, 1070.
(38) Bassi, I. W.; Scordamaglia, R. *J. Organomet. Chem.* **1972**, *37*, 353.
(39) De Cian, A.; L'Huillier, P. M.; Weiss, R. *Bull. Soc. Chim. Fr.* **1973**, 451.
(40) Kuźmina, L. G.; Struchkov, Yu. T.; Nekhaev, A. I. *Zh. Struct. Khim.* **1972**, *13*, 1115.
(41) Pierpont, C. G. *Inorg. Chem.* **1978**, *17*, 1976.
(42) Jones, R. O.; Maslen, E. N. *Z. Krist.* **1966**, *123*, 330.
(43) Der Piero, G.; Perego, G.; Cesari, M. *Gazz. Chim. Ital.* **1975**, *105*, 529.
(44) Tatsumi, K.; Yasuda, H.; Nakamura, A. *Isr. J. Chem.* **1983**, *23*, 145.
(45) Bunker, M. J.; Green, M. L. H. *J. Organomet. Chem.* **1980**, *192*, C6.
(46) Schilling, B. E. R.; Hoffmann, R.; Lichtenberger, D. L. *J. Am. Chem. Soc.* **1979**, *101*, 585 and references cited therein.

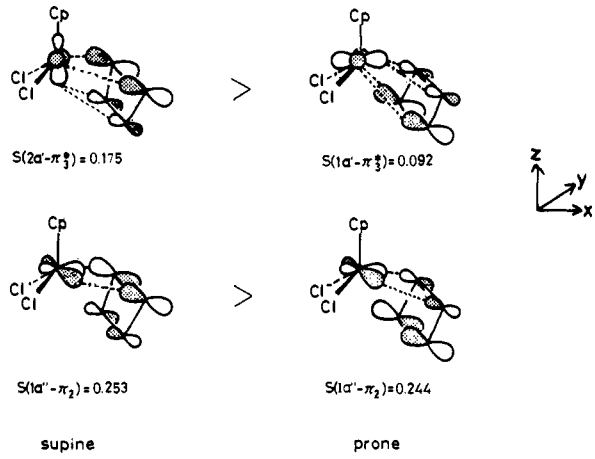

Figure 7. Schematic drawings of the two important interactions between the frontier orbitals of $CpTaCl_2$ (1a′, 2a′, 1a″) and butadiene π_2 and π_3^* in each rotamer of $CpTaCl_2(C_4H_6)$. Calculated overlap integrals S of each interaction are shown below the orbital sketch.

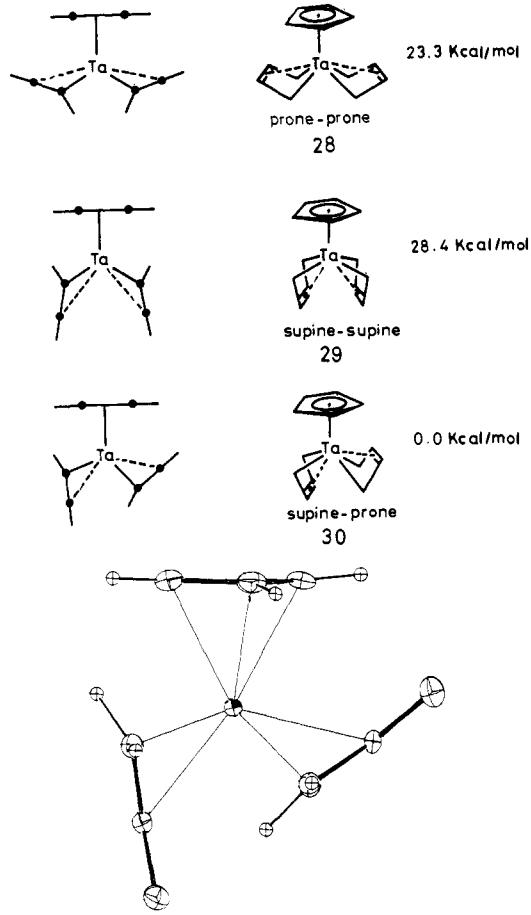

Figure 8. Side view of the optimized geometries for $CpTa(C_4H_6)_2$ in the three isomeric structures. The calculated total energies relative to the supine–prone geometry are given on the right. For a comparison, the side view of the X-ray structure obtained for $CpTa(C_6H_{10})_2$ is shown at the bottom.

thus smaller, lobes of π_2. Another consequence of the different $1a''-\pi_2$ interactions is that the Ta–C(terminal) bonds are more fully developed in supine, indicating a stronger 1,4-σ character of its Ta–C_4H_6 bonding. This will be important when we consider structural details of $CpTa(C_4H_6)_2$.

Next we turn to the electronic structure of bis(diene) complexes of Ta. The most intriguing aspect of these complexes is that two dienes adopt the supine–prone coordination[29] mode **30** shown in Figure 8 instead of the symmetrical structures **28** (prone–prone) and **29** (supine–supine). In an attempt to show relative stabilities,

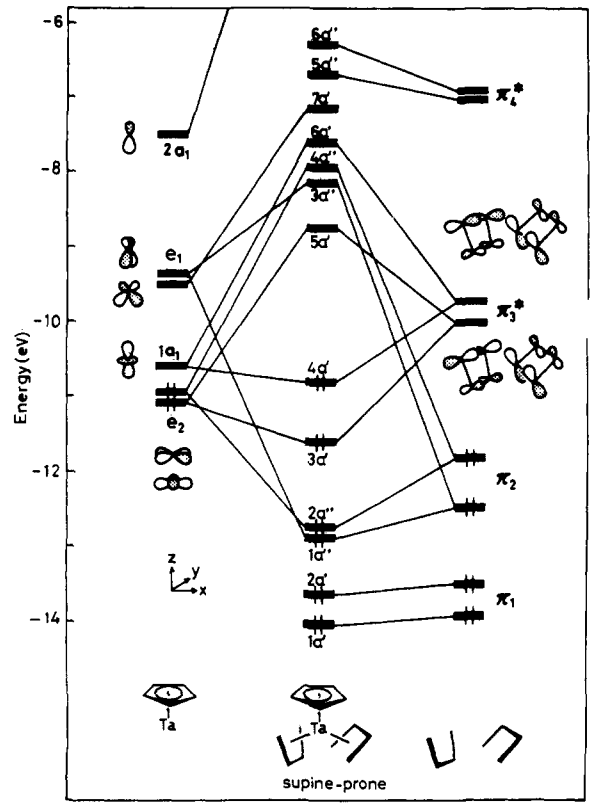

Figure 9. Orbital interaction diagram for $CpTa(C_4H_6)_2$ in the optimized supine–prone geometry. The molecular orbitals are assigned according to the molecular symmetry C_{5v} for CpTa and C_s for $CpTa(C_4H_6)_2$.

each structure of the molecule $CpTa(C_4H_6)_2$ was optimized as we did for $CpTaCl_2(C_4H_6)$. The Cp(centroid)–Ta–m angles for both butadienes were again fixed at 120°. Figure 8 shows side views of these optimized geometries on the left side; total energies are given at the extreme right. The conformation **30** (supine–supine) is clearly favored. The alternative conformers are much less stable in accord with the experimental observation. It should be mentioned that the side view of the theoretically optimized structure **30** is very close to that of the X-ray structure of $CpTa(C_6H_{10})_2$ shown at the bottom of Figure 8.

The supine–prone structure **30** is an interesting contrast to the more common supine–supine form of d^8 $Fe(CO)(C_4H_6)_2$,[26] d^8 $RhCl(C_4H_6)_2$,[27] and d^7 $Mn(L)(C_4H_6)_2$ [L = PR_3, CO].[28] Before discussing the electronic properties of **30**, we want to see whether in fact the extended-Hückel calculations can reproduce as well the "normal" supine–supine structure **29** for, e.g., $RhCl(C_4H_6)_2$. In determining geometries of the three isomers of $RhCl(C_4H_6)_2$, we again varied the parameters φ and L of **27** and chose a Cl–Rh–m angle of 120° for supine–supine and supine–prone and of 110° for prone–prone. Calculations do lead to a low energy for the supine–supine conformer (L = 0.9 Å, φ = 20°), being 27.2 kcal/mol and 25.9 kcal/mol lower than supine–prone (supine; L = 1.1 Å, φ = 25°: prone; L = 0.5 Å, φ = 20°) and prone–prone (L = 0.9 Å, φ = 20°), respectively. The molecular orbitals of $RhCl(supine\text{-}C_4H_6)_2$ resemble closely those of $Mn(PH_3)(supine\text{-}C_4H_6)_2$ obtained by Harlow et al.[28b] and are not shown in this paper.

Return to the interesting geometry of $CpTa(C_4H_6)_2$. Figure 9 shows interactions between CpTa orbitals and π (and π^*) of the two butadienes in the supine–prone conformation. The valence orbitals of CpM are well-known,[47] consisting of three relatively low-lying orbitals, $1a_1 + e_2$, and e_1 set at higher energy, and

(47) Lauher, J. W.; Elian, M.; Summerville, R. H.; Hoffmann, R. *J. Am. Chem. Soc.* **1976**, *98*, 3219 and references therein.

(48) The group notation is being changed in accord with recent actions by IUPAC and ACS nomenclature committees. A and B notation is being eliminated because of wide confusion. Group I becomes groups 1 and 11, group II becomes groups 2 and 12, group III becomes groups 3 and 13, etc.

another a_1 at still higher energy. The $1a_1$, e_2, and e_1 are mainly made of Ta d orbitals, with Ta p_x and p_y mixing in for e_1. The $2a_1$ is a hybrid of metal s, p_z, and z^2. These CpTa orbitals interact well with π orbitals of two butadienes. The set of π_2 orbital is stabilized by $xy(e_2)$ and $yz(e_1)$, which corresponds to the $1a''-\pi_2$ bonding of $CpTaCl_2(C_4H_6)$ as shown in Figure 9. The two π_3* orbitals also find partners to interact with, namely $z^2(1a_1)$ and $x^2-y^2(e_2)$. Interestingly, the latter interactions may be regarded as an assemblage of $2a'-\pi_3$* in **29** and $1a'-\pi_3$* in **28**. This is in fact why the molecule $CpTa(C_4H_6)_2$ and its derivatives choose the supine–prone conformations **30**. Only this conformation allows both π_3* orbitals to interact well with the low-lying z^2 and x^2-y^2 of CpTa. For the alternative symmetrical geometries, the higher orbital of the π_3* set does not overlap with either of them. The source of geometrical preference for **30** thus lies in the presence of two favorable interactions of the π_3* orbitals.

There is a better way of explaining the conformational choice. Taking advantage of the observed structure that coordination of 1,3-dienes to Ta has notable 1,4-σ-bond character, let us regard butadiene as a dianionic ligand as **31**. Then we consider that

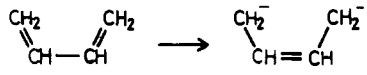

31

the Ta–butadiene bond comprises two Ta–C(terminal) σ bonds plus an interaction between Ta and the inner olefin portion. $CpTa(C_4H_6)_2$ carries four Ta–C σ bonds, forming a four-legged piano stool geometry **32**. The oxidation state of Ta is now

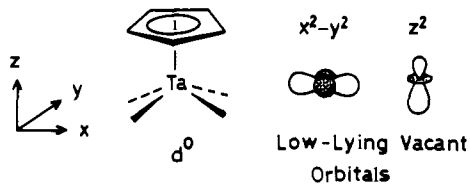

32

formally five and no d electron is available. Note that the electron count in the interaction diagram of Figure 9 assumes d^4 Ta with neutral butadienes. The difference in electron counting is a matter of formality and does not affect the theoretical results at all.

The bonds between Ta and two butadienes in $CpTa(C_4H_6)_2$ are completed when the inner olefin portion finds a way to interact with Ta. The d^0 piano stool molecule **32** has two low-lying vacant orbitals, x^2-y^2 and z^2,[13] which are potential acceptors of electrons from the occupied C–C π orbital of **31**. The $\pi-(x^2-y^2, z^2)$ donation interactions should be maximized if the two vacant orbitals are both utilized. This situation is achieved when one π system approaches the metal from the bottom and the other comes from the side as shown in **33**, thus leading to the conformation **30**. In

33

28 and **29**, the two π orbitals have to share one of these vacant d orbitals and the net interaction is significantly less than that in **30**.

We now look at each Ta–butadiene fragment in more detail. The X-ray structures of $CpTaCl_2(C_4H_6)$, $CpTa(C_6H_{10})_2$, and $Cp^*Ta(C_6H_{10})_2$ show that these complexes contain long–short–long C–C bonds in their diene skeletons and that the Ta–C(terminal) bond lengths are always shorter than the Ta–C(inner) ones. The observations imply the presence of 1,4-σ-bond character in the Ta–diene interactions. The Ta–C overlap populations calculated for the optimized geometries of $CpTaCl_2(C_4H_6)$ and $CpTa(C_4H_6)_2$ corroborate these trends. The numbers are summarized in Table VII. The Ta–C(1) (terminal) overlap populations are indeed larger than those of the Ta–C(2) (inner) bonds. Also found are the stronger C(2)–C(3) bonds compared with the C(1)–C(2) bonds. Then how significant is the 1,4-σ-bond character of these Ta complexes? Let us compare these with corresponding overlap populations calculated for $Fe(CO)_3(C_4H_6)$ and $Cp_2Zr(C_4H_6)$ in Table VII. $Fe(CO)_3(C_4H_6)$ is a classical example of η^4-butadiene complex, in which all carbon atoms of butadiene are almost equally involved in the bonding. On the other hand, $Cp_2Zr(C_4H_6)$ involves very strong Zr–C(terminal) bonds and concomitant weak Zr–C(inner) interactions. In the X-ray structure of $Cp_2Zr(C_6H_{10})$,[5a] the Zr–C(terminal) bond length of 2.300 Å is much shorter than the Zr–C(inner) distance of 2.597 Å. Should the difference between P[M–C(1)] and P[M–C(2)] be an indicator of the degree of 1,4-σ-bond character, the Ta butadiene complexes fall in between $Fe(CO)_3(C_4H_6)$ and $Cp_2Zr(C_4H_6)$. It may be worthy of note that 1,4-σ-bond character decreases as the central metal moves from left to right in the periodic table.

Table VII. Calculated Overlap Populations in $Fe(CO)_3(C_4H_6)$, $CpTaCl_2(C_4H_6)$, $CpTa(C_4H_6)_2$, and $Cp_2Zr(C_4H_6)$

	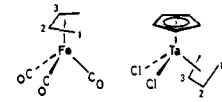		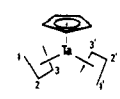		
P[M–C(1)]	0.202	0.289	0.296	0.264	0.338
P[M–C(2)]	0.184	0.108	0.074	0.120	0.060
P[C(1)–C(2)]	0.979	0.956	0.951	0.971	0.991
P[C(2)–C(3)]	0.974	1.037	1.058	1.012	1.012

Another point of interest that we have investigated includes the way in which two dienes coordinate to Ta in $CpTa(C_4H_6)_2$. The observed geometry of $CpTa(C_6H_{10})_2$ implies that the supine diene shows more pronounced 1,4-σ character than prone. The overlap populations computed for $CpTa(C_4H_6)_2$ very well reproduce this tendency. The electronic factors which differentiate the two Ta–butadiene bondings have something to do with the nature of interactions of π_2 and π_3* with CpTa orbitals. In the $xy-\pi_2$ bonding orbital 2a″, xy has better overlap with the terminal lobes of supine butadiene, than it does with the inner lobes in the prone geometry. Remember that π_2 has larger lobes at the terminal carbon atoms. This explanation is quite analogous to our analysis for $CpTaCl_2(C_4H_6)$ based on the $1a''-\pi_2$ interaction shown in Figure 7. There is one other factor which comes into play. Of the $(z^2, x^2-y^2)-\pi_3$* interactions, z^2 tends to overlap with the terminal lobes of prone, while x^2-y^2 directs toward those of supine. Thus the observed and calculated feature is partly due to the delicate balance between these two interactions. For $CpTa(C_4H_6)_2$, the x^2-y^2 interaction dominates.

On the other hand, the difference in C–C overlap populations between the terminal C(1)–C(2) (or C(3)–C(4)) bond and the inner C(2)–C(3) bond is more pronounced for the Ta complexes than $Cp_2Zr(C_4H_6)$. This result agrees quite well with the experimentally observed trend of Δl as shown in Figure 5b, but is opposite to what one might expect from a stronger 1,4-σ-bond character that $Cp_2Zr(C_4H_6)$ possesses. Roughly speaking, we may say that the 1,4-σ-bonding scheme accompanies a localization of double bond character at the inner C(2)–C(3) bond. However, nature is not always so obedient to such a simplistic picture, particularly so when one compares the delicate difference in bonding nature between the Ta and Zr complexes. Probably, the relative C–C bond strength or Δl of 1,3-dienes in metal complexes is not an accurate indicator of the 1,4-σ-bond nature.

Concluding Remarks

The salient features in bonding and the coordination geometry of $LTaCl_2$(diene) or $LTa(diene)_2$ (L = Cp, Cp*) have been

clarified on the basis of NMR and X-ray analyses coupled with theoretical treatments. These complexes are highly reactive toward aliphatic aldehydes and ketones and the 1:1 and/or 1:2 insertion reaction occurs selectively at the C(1) and/or C(4) atoms of the dienes to give unsaturated alcohol or glycols upon hydrolysis of the product. When the mixed-diene complex (**22**) is treated with an equivalent of a carbonyl compound, the insertion reaction takes place only at the butadiene ligand selectively. $CpTa(diene)_2$ is also reactive toward 1-alkynes such as 1-butyne and 1-hexyne. The addition of 3 equiv of 1-butyne to **9** or **10** results in the release of coordinated dienes at 60 °C and gives 1,3,5- and 1,2,4-triethylbenzene, a cyclic trimer of 1-butyne. Thus, Ta-diene complexes have unique chemical properties which promise a potential utility in organic synthesis and in homogeneous catalysis. Details of the reactions with these complexes will be given separately.

Acknowledgment. We thank Prof. N. Yasuoka of the Crystallographic Research Center for Protein Research, Osaka University, for affording the facilities of X-ray data measurement. Support of this study by a Grant-in-Aid for Special Project Research (No. 57218014) from the Ministry of Education, Science and Culture, Japan, is acknowledged.

Registry No. 3, 95250-97-8; **4**, 95250-98-9; **5**, 95250-99-0; **6**, 95251-00-6; 7, 95251-01-7; **8**, 95251-02-8; **9**, 95251-03-9; **10**, 95251-04-0; **11**, 95251-05-1; **12**, 95251-06-2; **13**, 95251-07-3; **22**, 95251-08-4; $CpTaCl_4$, 62927-98-4; Cp^*TaCl_4, 71414-47-6; $Fe(CO)_3(C_4H_6)$, 12078-32-9; $Cp_2Zr(C_4H_6)$, 75374-50-4; (2-butene-1,4-diyl)magnisium, 70809-00-6; (2-methyl-2-butene-1,4-diyl)magnisium, 90823-62-4; (2,3-dimethyl-2-butene-1,4-diyl)magnisium, 95251-09-5.

Supplementary Material Available: Tables of fractional atomic coordinates, equivalent isotropic temperature factors, anisotropic temperature factors for non-hydrogen and hydrogen atoms, and observed and calculated structure factors for complexes **3**, **10**, **13** (20 °C), and **13** (-60 °C) (141 pages). Ordering information is given on any current masthead page.

Olefin Isomerization Catalysis by Heterobimetallic Hydrides, $HFeM(CO)_8L^-$ (M = Cr, Mo, W; L = CO, PR_3)†

Patricia A. Tooley, Larry W. Arndt, and Marcetta Y. Darensbourg*

Contribution from the Department of Chemistry, Texas A&M University, College Station, Texas 77843. *Received August 3, 1984*

Abstract: The bis(triphenylphosphine)iminium (PPN^+) salts of $HFeM(CO)_9^-$ (M = Cr, Mo, W) were shown to be olefin isomerization catalysts under mild conditions (25 °C, fluorescent lighting) toward the conversion of allylbenzene to *cis*- and *trans*-propenylbenzenes and 1-hexene to internal olefins. When $DFeM(CO)_9^-$ was used as catalyst, deuterium label was incorporated into the isomerized products. The olefin isomerization capability of $HFe(CO)_4^-$ was reviewed. The $HFe(CO)_4^-$ anion is *inactive* in THF solution with PPN^+ as counterion, but activity may be generated in the presence of cocatalysts such as BF_3 and Ph_3C^+ (via a 1,3-shift mechanism) or alkali cations, Na^+ and Li^+ (via a reversible Fe-H addition mechanism). Evidence is presented which supports the action of the group 6 metal carbonyl fragment, $M(CO)_5^0$, to be similar to that of the alkali cations in promoting catalysis on the $Fe-H^-$ center.

Although the use of metal co-catalysts or promoters is prevalent throughout the literature of catalysis, their precise mechanistic role is generally poorly understood if at all. Developing from the approach, most convincingly articulated by Earl L. Muetterties,[1] of using polynuclear metal compounds as catalysts or catalyst models, the chemistry of discrete heterobimetallic complexes as models for mixed-metal catalysts is a growing field in organometallic chemistry.[2,3] In this connection we report herein the use of simple mixed-metal carbonyl hydrides, $HFeM(CO)_9^-$ (M = Cr, Mo, W),[4] as catalysts for olefin isomerization under mild conditions, of activity surpassing that of either parent homobimetallic hydride, $HFe_2(CO)_8^-$ or $HM_2(CO)_{10}^-$, or fragment components, $HFe(CO)_4^-$ or $M(CO)_5^0$.

The structure of $HFeW(CO)_9^-$ has been determined by X-ray crystallography.[4] The hydrogen atom could not be located; however, the relatively short Fe-W distance of 2.989 (2) Å (well within bonding range), coupled with one wide $(OC)_{eq}-Fe-(CO)_{eq}$ angle of 147.6 $(8)^0$, suggested the hydrogen to have considerable Fe-H terminal character. On the other hand, the distinctive high-field position of the hydride resonance (-11.8 ppm) and a definite (albeit small, 15 Hz) W-H coupling is consistent with at least some bridging hydride character.[4,5] Thus the structure of the heterobimetallic is quite different from that of the homobimetallic parents,[6,7] as illustrated in Figure 1. In fact, the extreme asymmetry of the "μ-H" ligand suggests the structure might be better visualized as a transition-metal Lewis acid, $M(CO)_5^0$, interacting with $HFe(CO)_4^-$ at electron density located on $Fe^{\delta-}$ or at the $Fe^{\delta-}-H$ bond density site:

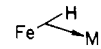

Another statement of this view is the $HFe(CO)_4^-$ moiety serves as an "18-electron complex ligand",[8] in occupancy of the sixth coordination site of $M(CO)_5^0$.

† The group notation is being changed in accord with recent actions by IUPAC and ACS nomenclature committees. A and B notation is being eliminated because of wide confusion. Group I becomes groups 1 and 11, group II becomes groups 2 and 12, group III becomes groups 3 and 13, etc.

(1) Muetterties, E. L. *Catal. Rev. Sci. Eng.* **1981**, *23*, 69.
(2) Casey, C. P.; Bullock, R. M.; Nief, F. *J. Am. Chem. Soc.* **1983**, *105*, 7574. Casey, C. P.; Bullock, R. M. *Organometallics* **1984**, *3*, 1100.
(3) Breen, M. J.; Shulman, P. M.; Geoffroy, G. L.; Rheingold, A. L.; Fultz, W. C. *Organometallics* **184**, *3*, 782.
(4) Arndt, L.; Delord, T.; Darensbourg, M. Y. *J. Am. Chem. Soc.* **1984**, *106*, 456.
(5) Several heterobimetallic hydrides of the type W-M(H) have been prepared and characterized, but in none of them was $^{183}W-H$ coupling detected: Breen, M. J.; Geoffroy, G. L.; Rheingold, A. L.; Fultz, W. C. *J. Am. Chem. Soc.* **1983**, *106*, 2638. Morrison, E. D.; Harley, A. D.; Marcelli, M. A.; Geoffroy, G. L.; Rheingold, A. L.; Fultz, W. C. *Organometallics* **1984**, *3*, 1407.
(6) Wilson, R. D.; Graham, S. A.; Bau, R. *J. Organomet. Chem.* **1975**, *91*, C49. Chin, H. B. Ph.D. Thesis, University of Southern California, Low Angeles, CA, 1975.
(7) (a) Collman, J. P.; Finke, R. G.; Matlock, P. L.; Wahren, R.; Komoto, R. G. *J. Am. Chem. Soc.* **1978**, *100*, 1119. (b) Sumner, C. Ph.D. Thesis, University of Texas, Austin, TX, 1981.
(8) Einstein, F. W. B.; Jones, T.; Pomeroy, R. K.; Rushman, P. *J. Am. Chem. Soc.* **1984**, *106*, 2707.

0002-7863/85/1507-2422$01.50/0